Shear deformable shell element DKMQ24 for composite structures

Irwan Katili, Imam Jauhari Maknun, Jean-Louis Batoz, Adnan Ibrahimbegovic

Shear deformable shell element DKMQ24 for composite structures

Irwan Katili[a],*, Imam Jauhari Maknun[a], Jean-Louis Batoz[b], Adnan Ibrahimbegovic[b]

[a] *Universitas Indonesia, Civil Engineering Department, Depok 16424, Indonesia*
[b] *Sorbonne University, Université de Technologie de Compiègne, UMR 6253 Roberval, 60205 Compiègne, France*

ARTICLE INFO

ABSTRACT

In this work we propose a new 4-node DKMQ24 shell element based on Naghdi-Reissner-Mindlin shell theory with 24 degrees of freedom. This new composite shell element, which is developed from DKMQ plate and shell elements, takes into account shear deformation, coupled bending-membrane energy and warping effects. This element has no spurious mode, passes patch tests for membrane, bending and shear problems. It has also successfully passed standard benchmark tests in the case of thick and thin shells without membrane and shear locking. In this paper, we extend the predictive capabilities of the DKMQ24 shell elements to composite laminated plates and shell structures. Numerical results obtained from DKMQ24 are compared against state-of-the-art shell elements. The results obtained by the proposed element converge more rapidly towards the reference solution.

1. Introduction

An ideal shell element for composite structures should be capable of modelling arbitrary shape of curved shell geometries and taking into account membrane, bending, couple membrane-bending and shear effects. The element formulation should be simple, avoiding whenever possible displacement derivatives as nodal variables, which require higher order continuity. Finally, it should be able to satisfy the rigid body and constant strain patch tests, be free of membrane and shear locking, as well as of spurious internal modes, be easily combined with other element types and able to provide accurate results for a coarse mesh.

The two main theories in shell analysis that are at our disposal for the theoretical formulation are the Kirchhoff-Love [1] and Naghdi-Reissner-Mindlin [2–7]. The first theory is only valid for thin shells and requires C^1 continuity, which is not easy to achieve for standard finite elements. For development of shell elements, it is thus easier to use the second theory, which requires only C^0 continuity. This theory, also known as shear deformable theory, is by far more popular for structural FEA (Finite Element Analysis).

The main challenge for low order Lagrange shell elements, based on Naghdi-Reissner-Mindlin hypothesis, concerns severe membrane and shear locking [8–11]. Locking cure has been an active domain of research, where several different methods have emerged. The simplest cure of reduced and selective integration techniques [12–22] can successfully reduce the numerical locking. The excessive bending stiffness of the fully integrated shell element is reduced, lowering the number of Gauss points in the numerical integration of the membrane and

transverse shear terms. However, reduced and selective integration can induce additional zero eigenvalues in the element stiffness matrix due to spurious modes in addition to the rigid body modes.

A more efficient cure is ANS (Assumed Natural Strains) [23–26] methods that exhibits better accuracy and robustness. The MITC4 (Mixed Interpolation of Tensorial Components) method has been effectively adopted for alleviating shear and membrane locking present in shell finite elements. The 4-node shell element MITC4 has been widely used in engineering practice due to its simple formulation and excellent performance [27]. A 3-node MITC3 shell element also is proposed [28], and this development is still being improved [29,30] with 3-nodes MITC3+ and MITC4+ elements. The DSG (Discrete Shear Gap) method developed by Bletzinger et al. to reduce shear locking [31] and the 3-node and 4-node DSG shell elements were also proposed. When used for plates, the 4-nodes DSG shell element formulation gives the MITC4 [27] element.

The development of 3-node DKT [32] and 4-node DKQ [33] elements for thick plate using ANS and Discrete Shear method to take into account the shear strains was proposed by Batoz and Lardeur [10,34,35]. These two elements rely on Reissner-Mindlin plate equilibrium equations to account for shear effects. The first one, called DST (Discrete Shear Triangular) [34], has 9 *d.o.f* and the second one, called DSQ (Discrete Shear Quadrilateral) [35] has 12 *d.o.f*. The numerical results of DST and DSQ elements converge towards those of DKT and DKQ plate elements for thin plate problems. Unfortunately, these two elements do not pass the patch test when applied to thick plate problem. To improve DST element, DST-BK has been proposed by Batoz and Katili [36] using free formulation method and incompatible modes.

---

* Corresponding author.
  E-mail address: irwan.katili@eng.ui.ac.id (I. Katili).

The element passes the patch tests when applied to thin and thick problems, and gives good and comparable results to DKT and DST.

A 4-nodes quadrilateral plate element called PQI with a set of incompatible modes is presented in [37–39]. In an analysis of thin plates, the element exhibits a similar performance as the well-known DKQ element. However, as opposed to the DKQ element, the element PQI can also be used successfully in an analysis of thick plates. Katili [40,41] also introduced DKMT and DKMQ elements to analyze thick and thin plate problems. These elements are based on Reissner-Mindlin [6,7] hypothesis, which requires only C^0 continuity. In the case of thin plate problems, the solutions obtained from DKMT element converge to DKT [32] element, while the solutions obtained from DKMQ element converge to DKQ [33] element. The problem of shear locking, when the thickness of the plate decreases, is resolved using the Discrete Kirchhoff Mindlin method, as proposed by Katili [40,41]. Therefore, DKMT and DKMQ elements are free of shear locking and passed the associated classical patch tests. The application of DKMQ plate element in stochastic finite element analysis, error estimation and buckling analysis were presented in [42–44]. The performance of DKMQ and DKMT plate element has been proved for thin and thick plate problems including composite plates [45,46]. Others papers in finite element for composite plates are found in [47–51]. Following the robustness of DKMQ plate element, 4-nodes DKMQ shell elements with 24 *dof* and 20 *dof* have been proposed [52–54].

A new development based on a modified Timoshenko beam theory and modified Reissner-Mindlin plate theory approach has been proposed recently for beam [55,56] and plate bending problems in isogeometric and finite element analysis [57–59]. Using unified and integrated (UI) approach [56,59], the total displacement is split into bending displacement and shear displacement which causes the rotations, curvatures and shear deformations can be defined as first, second and third derivatives of bending displacement, respectively. The shear-locking problem does not occur due to the strong interdependence among the bending displacement and rotations.

The main objective of this work is to build on our previous work [52] to study composite shell structures. The DKMQ24 shell element take into account coupled bending-membrane energy and warping effects. The DKMQ24 element passes the classical patch tests in thick and thin plate configurations, and the solutions converge quickly towards the reference values without shear locking. In this paper, we present a new development with DKMQ24 shell element for composite structures.

The paper is organized as follows. The geometry of shell element explained in Section 2. The constitutive laws at the level of a single laminate and at the stress resultant level are presented in Section 3 and 4, respectively. The shell kinematics for displacements and rotations are explained in Section 5. Furthermore, Section 6 presents the formulation of membrane deformation and curvatures strains, and Section 7 presents the assumed shear strain field. The element stiffness matrix including fictitious stiffness is explained in Sections 8 and 9. The numerical test results for composite plates and shells are shown in Section 10. In Section 11, we state the conclusions.

2. Geometric description of the DKMQ24 shell element

The geometry of the shell is defined with respect to a global Cartesian coordinate system *X, Y, Z* (Fig. 1) with associated unit vectors $\underset{\sim}{i}, \underset{\sim}{j}, \underset{\sim}{k}$ (Fig. 2). This system defines the directions for the global displacements *U, V, W* associated with the axes *X, Y, Z*, respectively. A nodal Cartesian coordinate system formed by unit vectors $\underset{\sim}{t}_{i1}, \underset{\sim}{t}_{i2}, \underset{\sim}{n}_i$ is defined at each node *i* on the reference surface (Fig. 2), see [11] for further detail.

The geometry of the shell is discretized by a mesh of quadrilateral elements with 4-nodes, which are not necessary in the same plane [52]. The position vector $\underset{\sim}{x}_p$ in the middle surface is continuous, but the direction of normal vector $\underset{\sim}{n}_i$ maybe discontinuous between two adjacent elements. The vector $\underset{\sim}{n}_i$ can be defined as the average of all the normal vectors at node *i,* corresponding to the elements attached to node *i*. This ensures geometric compatibility for coarse meshes and
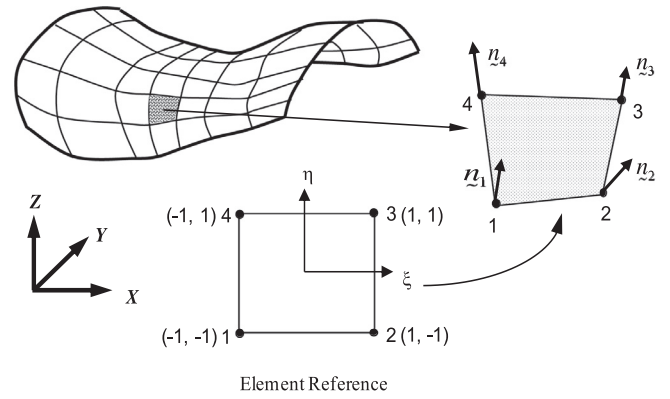

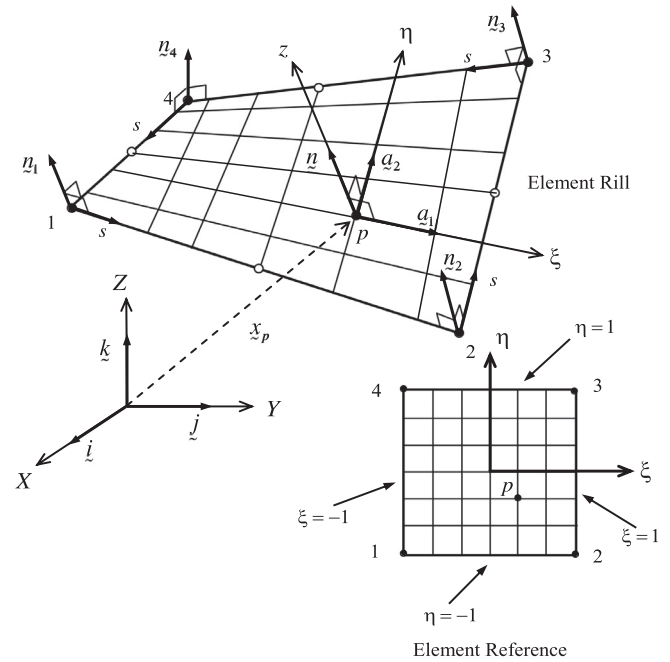**Fig. 1.** Shell geometry represented by a set of quadrilateral elements.

Fig. 2. Geometry of DKMQ24 shell element.

folded shells.

The interpolation of a position vector $\underset{\sim}{x}_q$ at an arbitrary point *q* is expressed as a function of the parametric coordinate ξ, η, z with z the thickness coordinate:

$$\underset{\sim}{x}_q(\xi,\eta,z) = \underset{\sim}{x}_p(\xi,\eta) + z\ \underset{\sim}{n}(\xi,\eta) \tag{1}$$

$$\underset{\sim}{x}_q(\xi,\eta,z) = \sum_{i=1}^{4} N_i(\xi,\eta)\ \underset{\sim}{x}_i + z\sum_{i=1}^{4} N_i(\xi,\eta)\ \underset{\sim}{n}_i \tag{2}$$

where:

$\underset{\sim}{x}_p$ is the position vector of an arbitrary point *p* in the middle surface with $z = 0$ in the global Cartesian coordinate system (*X, Y, Z*), which is defined in (ξ, η, z = 0).

$\underset{\sim}{x}_q$ is the position vector of an arbitrary point *q* (X_q, Y_q, Z_q) in the global Cartesian coordinate system, which is defined in (ξ, η, z ≠ 0).

$\underset{\sim}{x}_i$ is the coordinate of an arbitrary nodal *i* (X_i, Y_i, Z_i) in the global Cartesian coordinate system $\underset{\sim}{i}, \underset{\sim}{j}, \underset{\sim}{k}$. N_i (ξ,η) is the shape function of the quadrilateral element depending on the parametric coordinates (ξ, η) in the reference element (Table 1). $\underset{\sim}{n}_i$ denotes the normal direction at the surface of the shell element node *i* (Fig. 1).

Table 1
Linear function N_i and quadratic function P_k.

$N_1 = \frac{1}{4}(1-\xi)(1-\eta)$	$P_5 = \frac{1}{2}(1-\xi^2)(1-\eta)$
$N_2 = \frac{1}{4}(1+\xi)(1-\eta)$	$P_6 = \frac{1}{2}(1+\xi)(1-\eta^2)$
$N_3 = \frac{1}{4}(1+\xi)(1+\eta)$	$P_7 = \frac{1}{2}(1-\xi^2)(1+\eta)$
$N_4 = \frac{1}{4}(1-\xi)(1+\eta)$	$P_8 = \frac{1}{2}(1-\xi)(1-\eta^2)$

– *Local basis at* z = 0:

We define the covariant coordinate system by using the isoparametric coordinates for shell analysis. The relationship between differential elements in Cartesian and natural coordinates at point *p* can be written as

$$d\underset{\sim}{x}_p = \begin{Bmatrix} dX \\ dY \\ dZ \end{Bmatrix} = [\underset{\sim}{g}_1 \quad \underset{\sim}{g}_2] \begin{Bmatrix} d\xi \\ d\eta \end{Bmatrix} \tag{3}$$

Vectors $\underset{\sim}{g}_1$ and $\underset{\sim}{g}_2$ are tangential vectors in direction ξ and η. In general $\underset{\sim}{g}_1$ and $\underset{\sim}{g}_2$ are not orthogonal, and they are used to construct the *covariant basis*. Vectors $\underset{\sim}{g}_1$ and $\underset{\sim}{g}_2$ (Fig. 2) are given by

$$\underset{\sim}{g}_1 = \underset{\sim}{x}_{p,\xi} = \sum_{i=1}^{4} N_{i,\xi} \, \underset{\sim}{x}_i \; ; \; \underset{\sim}{g}_2 = \underset{\sim}{x}_{p,\eta} = \sum_{i=1}^{4} N_{i,\eta} \, \underset{\sim}{x}_i \tag{4}$$

where $N_{i,\xi}$ and $N_{i,\eta}$ are the first derivatives of the shape functions N_i with respect to ξ and η. The convention in this paper for $f_{,\xi}$ will denote the partial derivative of function f with respect to ξ.

The local basis at z = 0, denoted $[F_0]$, is written as:

$$[F_o] = [\underset{\sim}{g}_1 \, \underset{\sim}{g}_2 \, \underset{\sim}{n}]$$
$$det\,[F_o] = (\underset{\sim}{g}_1 \times \underset{\sim}{g}_2). \, \underset{\sim}{n} \; ; \; \underset{\sim}{n} = \frac{\underset{\sim}{g}_1 \times \underset{\sim}{g}_2}{|\underset{\sim}{g}_1 \times \underset{\sim}{g}_2|} \tag{5}$$

The length *ds* on the surface is classically given by:

$$(ds)^2 = d\underset{\sim}{x} \, . \, d\underset{\sim}{x} = \langle d\xi \; d\eta \rangle [a] \begin{Bmatrix} d\xi \\ d\eta \end{Bmatrix} \tag{6}$$

We denote by $[a]$ the *metric tensor* in the middle surface. It is a symmetric ($a_{12} = a_{21}$), positive-definite matrix defined as:

$$[a] = \begin{bmatrix} a_{11} & a_{12} \\ a_{21} & a_{22} \end{bmatrix} = \begin{bmatrix} \underset{\sim}{g}_1. \, \underset{\sim}{g}_1 & \underset{\sim}{g}_1. \, \underset{\sim}{g}_2 \\ \underset{\sim}{g}_2. \, \underset{\sim}{g}_1 & \underset{\sim}{g}_2. \, \underset{\sim}{g}_2 \end{bmatrix}$$
$$a = det\,[a]; \; a_{11} > 0 \; ; a_{22} > 0 \; ; \; det\,[a] > 0 \tag{7}$$

The area of element $d\underset{\sim}{A}$ expressed as:

$$d\underset{\sim}{A} = \underset{\sim}{g}_1 d\xi \times \underset{\sim}{g}_2 d\eta = |\underset{\sim}{g}_1 \times \underset{\sim}{g}_2| d\xi d\eta \, \underset{\sim}{n} \tag{8}$$

$$d\underset{\sim}{A} = \sqrt{a} \, d\xi d\eta \, \underset{\sim}{n} = dA \, \underset{\sim}{n} \; ; \; dA = \sqrt{a} \, d\xi \, d\eta \tag{9}$$

To simplify the calculations, we introduce the vectors $\underset{\sim}{g}^1$ and $\underset{\sim}{g}^2$ which are the classical *contravariant* vectors (Fig. 3). We recall that contravariant vectors satisfy:

$$\underset{\sim}{g}^1. \, \underset{\sim}{g}_1 = \underset{\sim}{g}^2. \, \underset{\sim}{g}_2 = 1 \; ; \underset{\sim}{g}^1. \, \underset{\sim}{g}_2 = \underset{\sim}{g}^2. \, \underset{\sim}{g}_1 = 0$$

The inverse matrix $[F_o]^{-1}$, with $[F_o]^{-1}[F_o] = [I]$, can be written as

$$[F_o]^{-T} = [\underset{\sim}{g}^1 \quad \underset{\sim}{g}^2 \quad \underset{\sim}{n}] \; and \; [\underset{\sim}{g}^1 \quad \underset{\sim}{g}^2] = [\underset{\sim}{g}_1 \quad \underset{\sim}{g}_2][a]^{-1} \tag{10}$$

The contravariant base vectors $\underset{\sim}{g}^1$ and $\underset{\sim}{g}^2$ are given by:

$$\underset{\sim}{g}^1 = \frac{1}{a}(a_{22} \, \underset{\sim}{g}_1 - a_{12} \, \underset{\sim}{g}_2) \; ; \; \underset{\sim}{g}^2 = \frac{1}{a}(-a_{21} \, \underset{\sim}{g}_1 + a_{11} \, \underset{\sim}{g}_2) \tag{11}$$

The relationship (3) can also be written in compact notation:

$$\begin{Bmatrix} d\xi \\ d\eta \end{Bmatrix} = \begin{bmatrix} \langle a^1 \rangle \\ \langle a^2 \rangle \end{bmatrix} \begin{Bmatrix} dX \\ dY \\ dZ \end{Bmatrix} \tag{12}$$

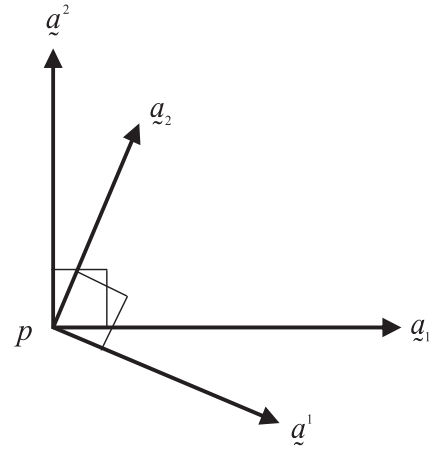The covariant and contravariant systems are important for

Fig. 3. Covariant and contravariant basis.

developing consistent expressions for the shell curvatures and the equilibrium equations in shell theory. The relation of differential calculation between global coordinate *X, Y, Z* and local coordinates system *x, y, z* can be written (Fig. 4) as:

$$\begin{Bmatrix} dX \\ dY \\ dZ \end{Bmatrix} = [Q] \begin{Bmatrix} dx \\ dy \\ dz \end{Bmatrix} \tag{13}$$

where:

$$[Q] = [\underset{\sim}{t}_1 \quad \underset{\sim}{t}_2 \quad \underset{\sim}{n}]$$
$$\underset{\sim}{t}_1 = \underset{\sim}{n} \times \underset{\sim}{k}; \; \underset{\sim}{t}_2 = \underset{\sim}{n} \times \underset{\sim}{t}_1; \; \underset{\sim}{t}_1 = \underset{\sim}{i} \; if \; \underset{\sim}{n} = \pm \underset{\sim}{k} \tag{14}$$

Relationships (12) and (13) become

$$\begin{Bmatrix} d\xi \\ d\eta \end{Bmatrix} = [C^o] \begin{Bmatrix} dx \\ dy \end{Bmatrix}, \; and$$

$$[C^o] = \begin{bmatrix} C_{11}^o & C_{12}^o \\ C_{21}^o & C_{22}^o \end{bmatrix} = \begin{bmatrix} \underset{\sim}{g}^1. \, \underset{\sim}{t}_1 & \underset{\sim}{g}^1. \, \underset{\sim}{t}_2 \\ \underset{\sim}{g}^2. \, \underset{\sim}{t}_1 & \underset{\sim}{g}^2. \, \underset{\sim}{t}_2 \end{bmatrix} \tag{15}$$

– *Local Basis at* z ≠ 0:

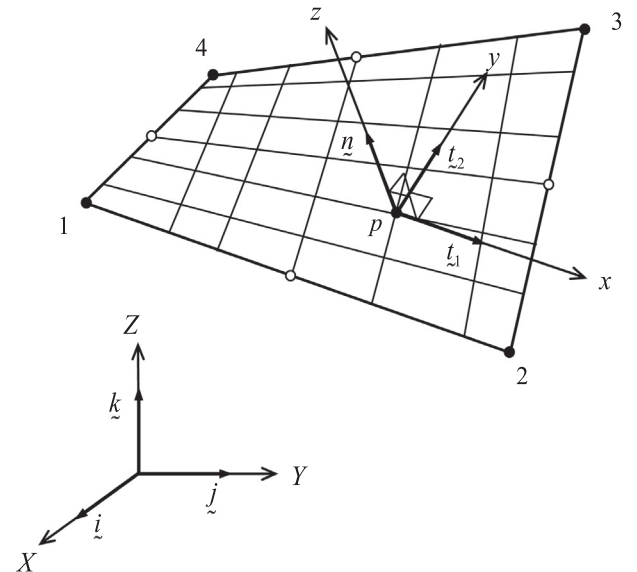The local basis $[F_z]$ at z ≠ 0 at an arbitrary point *q* outside of shell

Fig. 4. Local coordinate system *x, y, z* and global coordinate system *X, Y, Z*.

mid-surface can be written as:

$$[F_z] = [\underset{\sim}{g}_{1z} \quad \underset{\sim}{g}_{2z} \quad \underset{\sim}{n}] = [F_0] + z[F_n] \quad \text{where}$$

$$[F_n] = [\underset{\sim}{n}_{,\xi} \quad \underset{\sim}{n}_{,\eta} \quad \underset{\sim}{0}] \,; [F_z] = [F_0]([I] + z[b_n]) \tag{16}$$

With $[I]$ as the identity matrix, and

$$[b_n] = [F_0]^{-1}[F_n] \quad \text{or}$$

$$[b_n] = \begin{bmatrix} b_{n11} & b_{n12} & 0 \\ b_{n21} & b_{n22} & 0 \\ 0 & 0 & 0 \end{bmatrix} = \begin{bmatrix} \underset{\sim}{g}^1 \cdot \underset{\sim}{n}_{,\xi} & \underset{\sim}{g}^1 \cdot \underset{\sim}{n}_{,\eta} & 0 \\ \underset{\sim}{g}^2 \cdot \underset{\sim}{n}_{,\xi} & \underset{\sim}{g}^2 \cdot \underset{\sim}{n}_{,\eta} & 0 \\ 0 & 0 & 0 \end{bmatrix} \tag{17}$$

If the four nodes in an element are coplanar, then the matrix $[b_n]$ has a zero column because $\underset{\sim}{n}$ is constant in this element.

3. Constitutive laws

In local Cartesian coordinate systems (x, y, z), we can write the constitutive laws for in-plane stresses in each laminate as:

$$\{\sigma\} = [H]\{\varepsilon\} \tag{18}$$

where in-plane stresses are:

$$\{\sigma\} = \langle \sigma_x \quad \sigma_y \quad \sigma_{xy} \rangle^T \tag{19}$$

and membrane strain and curvatures are

$$\{\varepsilon\} = \{e\} + z\{\chi\}$$
$$\{e\} = \langle e_x \quad e_y \quad e_{xy} \rangle^T \,; \{\chi\} = \langle \chi_x \quad \chi_y \quad \chi_{xy} \rangle^T \tag{20}$$

The relation between out-off-plane shear stress and shear strain can be written as:

$$\{\tau\} = [G]\{\gamma\} \,; \{\tau\} = \langle \tau_x \quad \tau_y \rangle^T \text{ and} \{\gamma\} = \langle \gamma_x \quad \gamma_y \rangle^T \tag{21}$$

In the composite laminated shell structures, the material is formed by orthotropic layers with orthotropic axes *L-T-Z* and isotropic in the plane *TZ* (Fig. 5). The *L* axis defines the direction of the longitudinal fibres which are embedded in a matrix of polymeric or metallic material. Each layer satisfies the plane stress assumption ($\sigma_z = 0$). In each layer, the constitutive relationships in the orthotropic axes (*L-T-Z*) are:

$$\{\sigma_L\} = [H_L]\{\varepsilon_L\} \,; \{\tau_L\} = [G_L]\{\gamma_L\} \tag{22}$$

where:

$$\langle \sigma_L \rangle = \langle \sigma_L \quad \sigma_T \quad \sigma_{LT} \,; \langle \tau_L \rangle = \langle \tau_{LZ} \quad \tau_{TZ} \rangle$$
$$\langle \varepsilon_L \rangle = \langle \varepsilon_L \quad \varepsilon_T \quad 2\varepsilon_{LT} \,; \langle \gamma_L \rangle = \langle \gamma_{LZ} \quad \gamma_{TZ} \rangle \tag{23}$$

$$[H_L] = \begin{bmatrix} H_{LL} & H_{LT} & 0 \\ & H_{TT} & 0 \\ sym & & G_{LT} \end{bmatrix} \,; [G_L] = \begin{bmatrix} G_{LZ} & 0 \\ 0 & G_{TZ} \end{bmatrix} \tag{24}$$

$$H_{LL} = \frac{E_L}{(1 - \upsilon_{LT}\upsilon_{TL})} \,; \ H_{TT} = \frac{E_T}{(1 - \upsilon_{LT}\upsilon_{TL})}$$
$$H_{LT} = \frac{E_L\upsilon_{TL}}{(1 - \upsilon_{LT}\upsilon_{TL})} \,; \ E_T\upsilon_{LT} = E_L\upsilon_{TL} \tag{25}$$

The five independent coefficients can be either
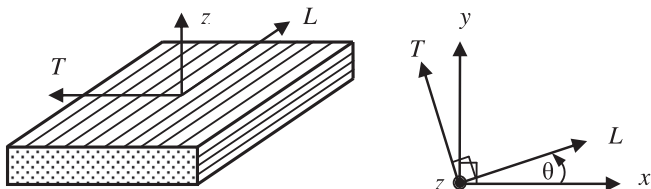
Fig. 5. Orthotropic layer.

$H_{LL}, H_{LT}, H_{TT}, \ G_{LT} = G_{LZ}, \ G_{TZ}$ or

$$E_L, E_T, \ \upsilon_{LT}\left(\text{or } \upsilon_{TL} \text{ with } \upsilon_{LT} = \frac{E_T\upsilon_{TL}}{E_L}\right),$$

$$G_{LT} = G_{LZ}, \ G_{TZ}\left(\text{or } \upsilon_{TZ} \text{ with } G_{TZ} = \frac{E_T}{2(1 + \upsilon_{TZ})}\right) \tag{26}$$

where E_L is the Young modulus in the fibre direction and E_T is the Young modulus in the transverse direction to the fibre, υ_{LT} and υ_{TL} are the Poisson ratios in the *L-T* plane of orthotropic layer. The constitutive parameters in matrices $[H_L]$ and $[G_L]$ can be measured experimentally. The orthotropic directions *L* and *T* can vary from layer to layer, and are represented by angle θ between the local axis *x* and the directions L_i of the ith layer (Fig. 5). The matrix transformation from orthotropic to local Cartesian coordinates can be written as

$$[R_{L1}] = \begin{bmatrix} C_\theta^2 & S_\theta^2 & C_\theta S_\theta \\ S_\theta^2 & C_\theta^2 & -C_\theta S_\theta \\ -2C_\theta S_\theta & 2C_\theta S_\theta & C_\theta^2 - S_\theta^2 \end{bmatrix}$$

$$\text{and:} \quad [R_{L2}] = \begin{bmatrix} C_\theta & S_\theta \\ -S_\theta & C_\theta \end{bmatrix}$$

$$\text{where:} \quad C_\theta = \cos\theta \,; S_\theta = \sin\theta \tag{27}$$

where: $[H] = [R_{L1}]^T[H_L][R_{L1}]$
$$[G] = [R_{L2}]^T[G_L][R_{L2}] \tag{28}$$

The last result can be simplified for the isotropic material

$$[H] = \frac{E}{1 - \upsilon^2} \begin{bmatrix} 1 & \upsilon & 0 \\ \upsilon & 1 & 0 \\ 0 & 0 & (1 - \upsilon)/2 \end{bmatrix}$$

$$[G] = \frac{E}{2(1 + \upsilon)} \begin{bmatrix} 1 & 0 \\ 0 & 1 \end{bmatrix} \tag{29}$$

where E is the Young modulus of elasticity, G is the shear modulus, υ the Poisson ratio.

4. Stress resultants

The stresses resultants are integral of the local Cartesian stress component σ_x, σ_y, σ_{xy}, τ_x and τ_y and given by:

$$N_x = \int_{-h/2}^{+h/2} \sigma_x dz \,; \ N_y = \int_{-h/2}^{+h/2} \sigma_y dz$$
$$N_{xy} = \int_{-h/2}^{+h/2} \sigma_{xy} dz \tag{30}$$

$$M_x = \int_{-h/2}^{+h/2} \sigma_x z \, dz \,; \ M_y = \int_{-h/2}^{+h/2} \sigma_y z \, dz$$
$$M_{xy} = \int_{-h/2}^{+h/2} \sigma_{xy} z \, dz \tag{31}$$

$$T_x = \int_{-h/2}^{+h/2} \tau_x dz \,; \ T_y = \int_{-h/2}^{+h/2} \tau_y dz \tag{32}$$

Where h is the shell thickness. The constitutive equations for the membrane forces, bending moments and shear forces, obtained from (18)–(32), are given by:

$$\begin{Bmatrix} N_x \\ N_y \\ N_{xy} \end{Bmatrix} = [H_m]\begin{Bmatrix} e_x \\ e_y \\ e_{xy} \end{Bmatrix} + [H_{mb}]\begin{Bmatrix} \chi_x \\ \chi_y \\ \chi_{xy} \end{Bmatrix}$$

$$\begin{Bmatrix} M_x \\ M_y \\ M_{xy} \end{Bmatrix} = [H_{mb}]\begin{Bmatrix} e_x \\ e_y \\ e_{xy} \end{Bmatrix} + [H_b]\begin{Bmatrix} \chi_x \\ \chi_y \\ \chi_{xy} \end{Bmatrix}$$

$$\begin{Bmatrix} T_x \\ T_y \end{Bmatrix} = [H_s]\begin{Bmatrix} \gamma_x \\ \gamma_y \end{Bmatrix} \tag{33}$$

For composite structures, the stress resultant constitutive equations are obtained by summing up over different layers. We thus obtain the stress resultant elasticity matrix for membrane and bending parts along with the membrane-bending coupling term due to non-symmetry of the
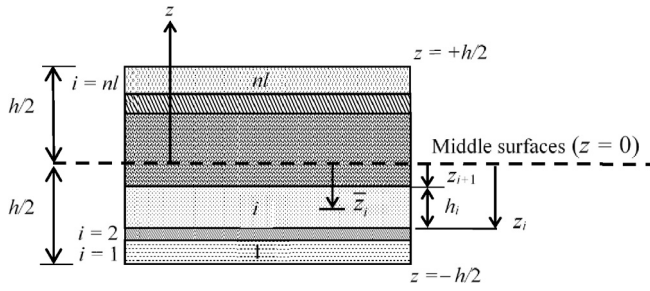
Fig. 6. Definition of layer in composite laminated shell.

composite shell, which are denoted as $[H_m]$, $[H_b]$, $[H_{mb}]$ and $[H_s]$ matrices (see Fig. 6).

Membrane constitutive matrix:

$$[H_m] = \begin{bmatrix} H_{m_{11}} & H_{m_{12}} & H_{m_{13}} \\ & H_{m_{22}} & H_{m_{23}} \\ Sym. & & H_{m_{33}} \end{bmatrix} = \sum_{i=1}^{nl} [H]_i h_i$$

$$h_i = (z_{i+1} - z_i) \tag{34}$$

Bending constitutive matrix:

$$[H_b] = \begin{bmatrix} H_{b_{11}} & H_{b_{12}} & H_{b_{13}} \\ & H_{b_{22}} & H_{b_{23}} \\ Sym. & & H_{b_{33}} \end{bmatrix} = \frac{1}{3} \sum_{i=1}^{nl} [H]_i (z_{i+1}^3 - z_i^3) \tag{35}$$

Coupled membrane-bending constitutive matrix:

$$[H_{mb}] = \begin{bmatrix} H_{mb_{11}} & H_{mb_{12}} & H_{mb_{13}} \\ & H_{mb_{22}} & H_{mb_{23}} \\ Sym. & & H_{mb_{33}} \end{bmatrix} = \frac{1}{2} \sum_{i=1}^{nl} [H]_i h_i \bar{z}_i$$

$$h_i = z_{i+1} - z_i \; ; \; \bar{z}_i = \frac{1}{2}(z_{i+1} + z_i) \tag{36}$$

where h_i is the layer thickness.

If the material properties and the laminate orientations are symmetric with respect to the middle surface, $[H_{mb}]$ is zero and the middle surface xy is a neutral surface. Middle surface xy then coincides with the neutral surface and the membrane and bending effects are uncoupled. This means that in-plane forces acting on neutral surface do not produces any curvatures and, conversely, bending moments do not produce any membrane strain.

Shear constitutive matrix:

$$[\bar{H}_s] = \begin{bmatrix} \bar{H}_{s_{11}} & \bar{H}_{s_{12}} \\ Sym. & \bar{H}_{s_{22}} \end{bmatrix} = \sum_{i=1}^{nl} [G]_i h_i$$

$$h_i = (z_{i+1} - z_i) \tag{37}$$

where nl is the number of layers in the structures. $[H]_i$ is the in-plane constitutive matrix for i^{th} layer and $[G]_i$ is the out-of-plane constitutive matrix for i^{th} layer. They are defined in (28) for orthotropic material and in (29) for isotropic material. Matrix $[H_s]$ is defined so that the shear strain energy density obtained for an exact 3D distribution of the transverse shear stresses τ_x and τ_y is identical to the shear energy associated with the Naghdi-Reissner-Mindlin plate model. The requirement that the transverse shear stiffness of the shell model should correspond as much as possible with respect to the one from 3D analysis is met by using the modified constitutive matrix $[H_s]$ for the shear forces (37) which can be written as

$$[H_s] = \begin{bmatrix} \kappa_{11}. \bar{H}_{s_{11}} & \kappa_{12}. \bar{H}_{s_{12}} \\ Sym. & \kappa_{22}. \bar{H}_{s_{22}} \end{bmatrix} \tag{38}$$

where κ_{11}, κ_{12}, κ_{22} are the transverse shear correction parameters.

For isotropic material, we can simplify these constitutive matrices. The matrix $[H_m]$, $[H_b]$ and $[H_s]$ are then given by:

$$[H_m] = D_m \begin{bmatrix} 1 & \upsilon & 0 \\ \upsilon & 1 & 0 \\ 0 & 0 & (1-\upsilon)/2 \end{bmatrix} ; D_m = \frac{Eh}{(1-\upsilon^2)} \tag{39}$$

$$[H_b] = D_b \begin{bmatrix} 1 & \upsilon & 0 \\ \upsilon & 1 & 0 \\ 0 & 0 & (1-\upsilon)/2 \end{bmatrix} ; D_b = \frac{Eh^3}{12(1-\upsilon^2)} \tag{40}$$

$$[H_{mb}] = [0] \tag{41}$$

$$[H_s] = D_s \begin{bmatrix} 1 & 0 \\ 0 & 1 \end{bmatrix} ; D_s = \kappa Gh \tag{42}$$

For the isotropic material we typically chose $\kappa = 5/6$, which is computed as the transverse shear correction parameters of (38) based on considerations of static equivalences [10].

5. Kinematics of DKMQ24 shell element

There are 24 degrees of freedom on each element, three displacements and three rotations at each node i (U_i, V_i, W_i, θ_{X_i}, θ_{Y_i}, θ_{Z_i}) in the global coordinates system (Fig. 7).

For the approximation of displacement in the middle surface, $\underset{\sim}{u}_p(\xi,\eta)$, the element uses a linear function. For the interpolation of rotations $\underset{\sim}{\beta}(\xi,\eta)$, DKMQ24 uses an incomplete quadratic polynomial. The displacement of point outside mid-surface $\underset{\sim}{u}_q$ can then be written as [52]

$$\underset{\sim}{u}_q(\xi,\eta,z) = \underset{\sim}{u}_p(\xi,\eta) + z\underset{\sim}{\beta}(\xi,\eta) \quad \text{with: } \underset{\sim}{\beta} \cdot \underset{\sim}{n} = 0 \tag{43}$$

where mid-surface displacement is bi-linear:

$$\underset{\sim}{u}_p(\xi,\eta) = \sum_{i=1}^{4} N_i(\xi,\eta) \begin{Bmatrix} U_i \\ V_i \\ W_i \end{Bmatrix} \tag{44}$$

The rotation approximation for $\underset{\sim}{\beta}$ is incomplete bi-quadratic function.

$$\underset{\sim}{\beta}(\xi,\eta) = \sum_{i=1}^{4} N_i(\xi,\eta)\underset{\sim}{\beta}_i + \sum_{k=5}^{8} P_k(\xi,\eta) \underset{\sim}{t}_{sk} \Delta\beta_{sk}$$

$$\underset{\sim}{\beta}_i = \underset{\sim}{\theta}_i \times \underset{\sim}{n}_i \; ; \; \underset{\sim}{t}_{sk} = \frac{\underset{\sim}{x}_{ji}}{L_k} = \frac{(\underset{\sim}{x}_j - \underset{\sim}{x}_i)}{L_k} \tag{45}$$
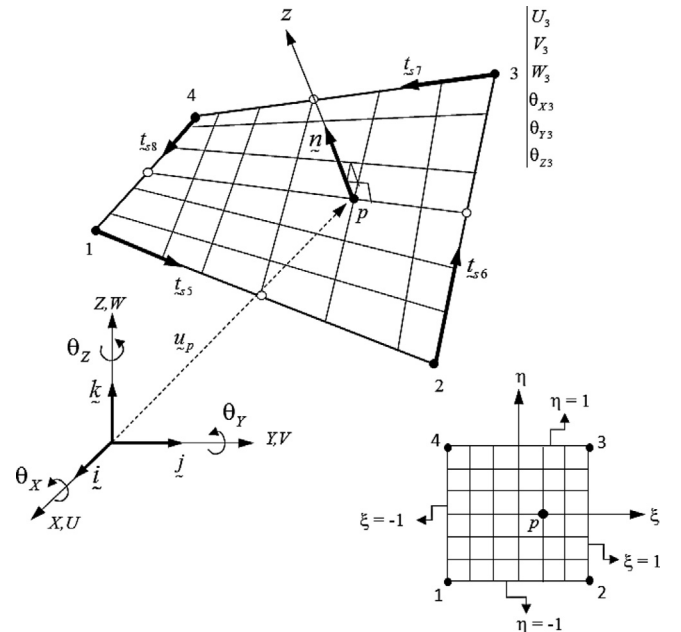

Fig. 7. Nodal degrees of freedom for DKMQ24 shell elements.

$$\underset{\sim}{\beta} = \sum_{i=1}^{4} N_i [RN]_i \begin{Bmatrix} \theta_{X_i} \\ \theta_{Y_i} \\ \theta_{Z_i} \end{Bmatrix} + \sum_{k=5}^{8} P_k \underset{\sim}{t}_{s_k} \Delta\beta_{s_k} \tag{46}$$

$$[RN]_i = [\{RN1\}_i \ \ \{RN2\}_i \ \ \{RN3\}_i] = \begin{bmatrix} 0 & n_{Zi} & -n_{Yi} \\ -n_{Zi} & 0 & n_{Xi} \\ n_{Yi} & -n_{Xi} & 0 \end{bmatrix} \tag{47}$$

where N_i is a linear function and P_k is a quadratic function (see Table 1); $\Delta\beta_{s_k}$ ($k = 5, 6, 7, 8$) is a supplementary degree of freedom on each side of the element, which represents a hierarchical rotation with respect to the average of β_{s_i} and β_{s_j} in the middle of each side (Fig. 8), L_k is the length of side $i\text{-}j$.

The rotation components β_s and β_m are defined according;

$$\beta_s = \underset{\sim}{\beta} \cdot \underset{\sim}{t}_{s_k}; \ \ \beta_m = \underset{\sim}{\beta} \cdot \underset{\sim}{t}_{m_k}; \ \ \underset{\sim}{t}_{m_k} = \underset{\sim}{t}_{s_k} \wedge \underset{\sim}{n}_k \tag{48}$$

where $\underset{\sim}{t}_{s_k}$ and $\underset{\sim}{t}_{m_k}$ ($k = 5, 6, 7, 8$) are the unit vector tangential and normal to the side of k (Fig. 9). We note the rotation β_s (in the plane $z\text{-}s$, where s is the tangential coordinate on the considered side of $i\text{-}j$) is a quadratic function with respect to s. The rotation component β_m (in the plane $z\text{-}m$ where m is perpendicular to s and $\underset{\sim}{n}$) is a linear function in s (Fig. 8). For example, along the side of $i\text{-}j$, we have

$$\beta_s = \left(1 - \frac{s}{L_k}\right)\beta_{s_i} + \frac{s}{L_k}\beta_{s_j} + 4\frac{s}{L_k}\left(1 - \frac{s}{L_k}\right)\Delta\beta_{s_k}$$

$$\beta_m = \left(1 - \frac{s}{L_k}\right)\beta_{m_i} + \frac{s}{L_k}\beta_{m_j} \tag{49}$$

6. Approximation of membrane strains and curvatures

We take from [52] the approximation for membrane strains which can be written as

$$\{e\} = \begin{Bmatrix} e_x \\ e_y \\ e_{xy} \end{Bmatrix} = \begin{bmatrix} \underset{\sim}{t}_1 & 0 \\ 0 & \underset{\sim}{t}_2 \\ \underset{\sim}{t}_2 & \underset{\sim}{t}_1 \end{bmatrix} [C^o]^T \begin{Bmatrix} \underset{\sim}{u}_{p,\xi} \\ \underset{\sim}{u}_{p,\eta} \end{Bmatrix} \tag{50}$$

By introducing (44) into (50), we get:

$$\{e\} = [B_m]\{u_n\} \tag{51}$$

$$\{u_n\} = <\ ...\ U_i\ V_i\ W_i\ \theta_{X_i}\ \theta_{Y_i}\ \theta_{Z_i}\ ...\ >_{i=1,4}^T \tag{52}$$

and

$$[B_m] = [\cdots \ [B_m]_i \ \cdots]_{i=1,4}$$

$$[B_m]_i = \begin{bmatrix} \langle t_1 \rangle N_{i,x} & 0 & 0 & 0 \\ \langle t_2 \rangle N_{i,y} & 0 & 0 & 0 \\ \langle t_1 \rangle N_{i,y} + \langle t_2 \rangle N_{i,x} & 0 & 0 & 0 \end{bmatrix} \tag{53}$$

$$N_{i,x} = N_{i,\xi} C_{11}^o + N_{i,\eta} C_{21}^o$$
$$N_{i,y} = N_{i,\xi} C_{12}^o + N_{i,\eta} C_{22}^o \tag{54}$$

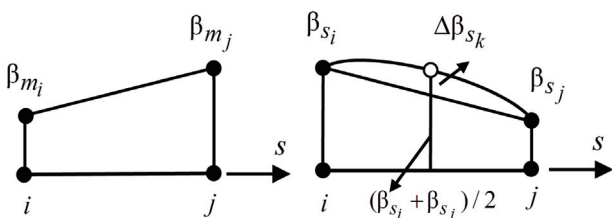The approximation for components of the curvature tensor is given by:

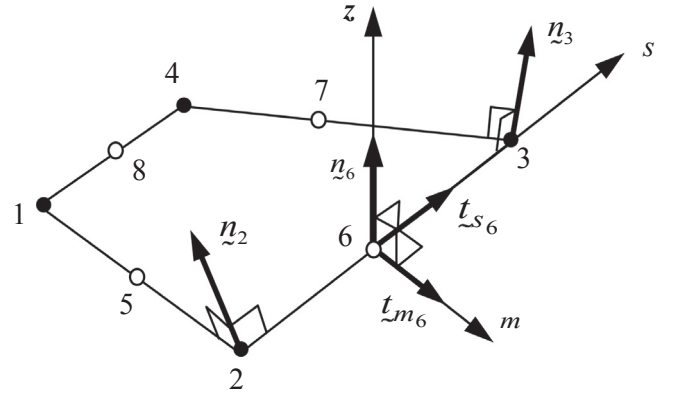**Fig. 8.** Variation of rotation β_m and β_s along the sides of DKMQ24 shell element.

Fig. 9. Tangential unit vector on side $i\text{-}j$.

$$\{\chi\} = \begin{Bmatrix} \chi_x \\ \chi_y \\ \chi_{xy} \end{Bmatrix} = \begin{bmatrix} \underset{\sim}{t}_1 & 0 \\ 0 & \underset{\sim}{t}_2 \\ \underset{\sim}{t}_2 & \underset{\sim}{t}_1 \end{bmatrix} \left[[bc]^T \begin{Bmatrix} \underset{\sim}{u}_{p,\xi} \\ \underset{\sim}{u}_{p,\eta} \end{Bmatrix} + [C^o]^T \begin{Bmatrix} \underset{\sim}{\beta}_{,\xi} \\ \underset{\sim}{\beta}_{,\eta} \end{Bmatrix} \right] \tag{55}$$

By introducing (44)–(48) into (55), we get

$$\{\chi\} = [B_{b_\beta}]\{u_n\} + [B_{b_{\Delta\beta}}]\{\Delta\beta_n\} \tag{56}$$

where

$$\langle \Delta\beta_n \rangle = \langle \Delta\beta_{s_5} \ \ \Delta\beta_{s_6} \ \ \Delta\beta_{s_7} \ \ \Delta\beta_{s_8} \rangle \tag{57}$$

$$[B_{b_\beta}] = [\cdots \ [B_{b_\beta}]_i \ \cdots]_{i=1,4}$$

$$[B_{b_\beta}]_i = \begin{bmatrix} \langle t_1 \rangle Nbc1_i & \langle V1_i \rangle N_{i,x} \\ \langle t_2 \rangle Nbc2_i & \langle V2_i \rangle N_{i,y} \\ \langle t_1 \rangle Nbc2_i + \langle t_2 \rangle Nbc1_i & \langle V1_i \rangle N_{i,y} + \langle V2_i \rangle N_{i,x} \end{bmatrix} \tag{58}$$

$$\langle V1_i \rangle = \ < \underset{\sim}{t}_1 \cdot \underset{\sim}{RN}_{1_i} \ \ \underset{\sim}{t}_1 \cdot \underset{\sim}{RN}_{2_i} \ \ \underset{\sim}{t}_1 \cdot \underset{\sim}{RN}_{3_i} >$$
$$\langle V2_i \rangle = \ < \underset{\sim}{t}_2 \cdot \underset{\sim}{RN}_{1_i} \ \ \underset{\sim}{t}_2 \cdot \underset{\sim}{RN}_{2_i} \ \ \underset{\sim}{t}_2 \cdot \underset{\sim}{RN}_{3_i} > \tag{59}$$

$$Nbc1_i = N_{i,\xi} bc_{11} + N_{i,\eta} bc_{21}; \ \ Nbc2_i = N_{i,\xi} bc_{12} + N_{i,\eta} bc_{22} \tag{60}$$

$$[B_{b_{\Delta\beta}}] = \begin{bmatrix} & \underset{\sim}{t}_1 \cdot \underset{\sim}{t}_{s_k} P_{k,x} & \\ \cdots & \underset{\sim}{t}_2 \cdot \underset{\sim}{t}_{s_k} P_{k,y} & \cdots \\ & \underset{\sim}{t}_1 \cdot \underset{\sim}{t}_{s_k} P_{k,y} + \underset{\sim}{t}_2 \cdot \underset{\sim}{t}_{s_k} P_{k,x} & \end{bmatrix}_{k=5,8} \tag{61}$$

$$P_{k,x} = P_{k,\xi} C_{11}^o + P_{k,\eta} C_{21}^o; \ \ P_{k,y} = P_{k,\xi} C_{12}^o + P_{k,\eta} C_{22}^o \tag{62}$$

From [52] we have:

$$[bc] = \begin{bmatrix} bc_{11} & bc_{12} \\ bc_{21} & bc_{22} \end{bmatrix} = \ [\hat{b}][C^o]$$

$$[\hat{b}] = \begin{bmatrix} b_{n22} & -b_{n12} \\ -b_{n21} & b_{n11} \end{bmatrix} = \begin{bmatrix} \underset{\sim}{a}^2 \cdot \underset{\sim}{n}_{,\eta} & -\underset{\sim}{a}^1 \cdot \underset{\sim}{n}_{,\eta} \\ -\underset{\sim}{a}^2 \cdot \underset{\sim}{n}_{,\xi} & \underset{\sim}{a}^1 \cdot \underset{\sim}{n}_{,\xi} \end{bmatrix} \tag{63}$$

We can see that there is a coupling between bending and membrane for the curvature strains equations in (58). This happens if the four nodes in the element are not coplanar $[bc] \neq [0]$. If the four nodes in an element are coplanar, then the matrix $[bc] = [0]$ (because $\underset{\sim}{n}$ is constant for this element). In this situation the formulation will give the same results as with the flat shell model.

7. Assumed shear strain fields for DKMQ24

The key point of formulation for shear locking free in the case of composite shell structures is the choice of the assumed shear strain field. We briefly present the assumed strain fields used in the DKMQ24 shell element. The main reason for that concerns the importance of shear deformation with respect to the risk of shear failure in

composites. Shear strain field is approximated independently of displacement and rotations in the spirit of assumed shear strain. Due to the element curvature, it is convenient to express the assumed shear strain field in the covariant components $\underline{\gamma}_\xi$ and $\underline{\gamma}_\eta$, and then transform the resulting expressions to the local coordinate system.

The definition of the assumed shear strain field $\{\underline{\gamma}\}$ follows similar arguments to that for our plate and shell elements [41,52]. Namely given construction in the covariant system, we obtain the corresponding approximation in the local Cartesian system.

$$\{\underline{\gamma}\} = \begin{Bmatrix} \underline{\gamma}_x \\ \underline{\gamma}_y \end{Bmatrix} = [C^o]^T \begin{Bmatrix} \underline{\gamma}_\xi \\ \underline{\gamma}_\eta \end{Bmatrix} = \begin{bmatrix} C_{11}^o & C_{12}^o \\ C_{21}^o & C_{22}^o \end{bmatrix} \begin{Bmatrix} \underline{\gamma}_\xi \\ \underline{\gamma}_\eta \end{Bmatrix} \tag{64}$$

Following the choice in [41,52], we take covariant shear component approximation

$$\begin{Bmatrix} \underline{\gamma}_\xi \\ \underline{\gamma}_\eta \end{Bmatrix} = [N_\gamma]\{\underline{\gamma}_{\xi n}\}$$

$$\begin{Bmatrix} \underline{\gamma}_\xi \\ \underline{\gamma}_\eta \end{Bmatrix} = \begin{bmatrix} \frac{1}{2}(1-\eta) & 0 & \frac{1}{2}(1+\eta) & 0 \\ 0 & \frac{1}{2}(1+\xi) & 0 & \frac{1}{2}(1-\xi) \end{bmatrix} \begin{Bmatrix} \underline{\gamma}_{\xi 5} \\ \underline{\gamma}_{\eta 6} \\ \underline{\gamma}_{\xi 7} \\ \underline{\gamma}_{\eta 8} \end{Bmatrix} \tag{65}$$

where $\underline{\gamma}_{\xi 5}, \underline{\gamma}_{\eta 6}, \underline{\gamma}_{\xi 7}, \underline{\gamma}_{\eta 8}$ denote the natural shear strains at the mid-points of the element sides 5,6,7,8. On the other hand, we can replace these covariant components with the corresponding physical components simply by using the correct metric for each element side

$$\begin{Bmatrix} \underline{\gamma}_{\xi 5} \\ \underline{\gamma}_{\eta 6} \\ \underline{\gamma}_{\xi 7} \\ \underline{\gamma}_{\eta 8} \end{Bmatrix} = \frac{1}{2} \begin{bmatrix} L_5 & 0 & 0 & 0 \\ 0 & L_6 & 0 & 0 \\ 0 & 0 & -L_7 & 0 \\ 0 & 0 & 0 & -L_8 \end{bmatrix} \begin{Bmatrix} \underline{\gamma}_{s5} \\ \underline{\gamma}_{s6} \\ \underline{\gamma}_{s7} \\ \underline{\gamma}_{s8} \end{Bmatrix} = [A_\gamma]\{\underline{\gamma}_{sn}\} \tag{66}$$

With the results (64)–(66) on hand, we obtain:

$$\{\underline{\gamma}\} = [B_{s\gamma}]\{\gamma_{sn}\}$$
$$[B_{s\gamma}] = [C^o]^T [N_\gamma][A_\gamma] \tag{67}$$

Thus the assumed independent shear strain $\underline{\gamma}_s$ on side-k (k = 5, 6, 7, 8) (Fig. 10), can be expressed as:

$$\underline{\gamma}_{s_k} = -\frac{2}{3}\phi_k\Delta\beta_{s_k} \tag{68}$$

where the coefficient ϕ_k can be obtained for either orthotropic material [45]

$$\phi_k = (H_{s k_{21}}^{inv} H_{b_{k32}} + H_{s k_{22}}^{inv} H_{b_{k22}})\left(\frac{12}{L_k^2}\right) \tag{69}$$

where L_k is the length of the side k, and

$$[H_{b_k}] = [R_{k_1}]^T [H_b][R_{k_1}]$$
$$[H_{s_k}] = [R_{k_2}]^T [H_s][R_{k_2}] \; ; \; [H_{s_k}^{inv}] = [H_{s_k}]^{-1} \tag{70}$$

where $[R_{k_1}]$ and $[R_{k_2}]$ are given by:

$$[R_{k_1}] = \begin{bmatrix} S_k^2 & C_k^2 & S_k C_k \\ C_k^2 & S_k^2 & -S_k C_k \\ -2S_k C_k & 2S_k C_k & S_k^2 - C_k^2 \end{bmatrix}$$

$$[R_{k_2}] = \begin{bmatrix} S_k & C_k \\ -C_k & S_k \end{bmatrix} ; \begin{Bmatrix} C_k \\ S_k \end{Bmatrix} = \begin{Bmatrix} \underline{t}_1 \cdot \underline{t}_{s_k} \\ \underline{t}_2 \cdot \underline{t}_{s_k} \end{Bmatrix} \tag{71}$$

or for an isotropic material [41]

$$\phi_k = \frac{D_b}{D_s}\frac{12}{L_k^2} = \frac{2}{\kappa(1-\upsilon)}\left(\frac{h^2}{L_k^2}\right) \tag{72}$$

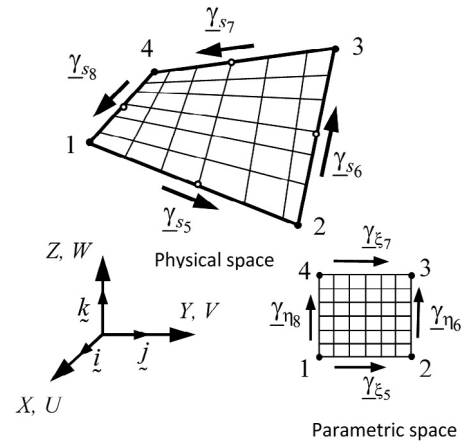The factor ϕ_k, characterizing the influence of shear, maintains the

Fig. 10. Constant assumed shear strain on side *i-j*.

consistency of the proposed element. The factor ϕ_k in the above equation precisely explains why DKMQ24 element behaves as either *Reissner-Mindlin* theory for thick shell or as *Kirchhoff-Love* theory for thin shell. In the thin shell problems, where factor ϕ_k is close to zero, shear deformation is automatically reduced. Accordingly, as the main positive result, the *shear locking* is automatically resolved by this Discrete Kirchhoff Mindlin method. Applying the same procedure systematically on all sides of the proposed shell element, from Eq. (68) we get [41,52]

$$\begin{Bmatrix} \underline{\gamma}_{s5} \\ \underline{\gamma}_{s6} \\ \underline{\gamma}_{s7} \\ \underline{\gamma}_{s8} \end{Bmatrix} = -\frac{2}{3} \begin{bmatrix} \phi_5 & 0 & 0 & 0 \\ 0 & \phi_6 & 0 & 0 \\ 0 & 0 & \phi_7 & 0 \\ 0 & 0 & 0 & \phi_8 \end{bmatrix} \begin{Bmatrix} \Delta\beta_{s5} \\ \Delta\beta_{s6} \\ \Delta\beta_{s7} \\ \Delta\beta_{s8} \end{Bmatrix}$$
$$\{\underline{\gamma}_{sn}\} = [A_\phi]\{\Delta\beta_n\} \tag{73}$$

Finally, combining (67) and (73) we obtain:

$$\{\underline{\gamma}\} = \begin{Bmatrix} \underline{\gamma}_x \\ \underline{\gamma}_y \end{Bmatrix} = \begin{bmatrix} B_{s\gamma} \end{bmatrix}[A_\phi]\{\Delta\beta_n\} \tag{74}$$

8. Variational principal and shell element stiffness matrix

The modified *Hu-Washizu* functional is used as the appropriate framework to develop our DKMQ24 shell element. We only briefly recall the modified *Hu-Washizu* principle, whose details can be found in Refs. [60,61]. The Hu-Washizu principle for shell can be written as:

$$\Pi = \Pi_{int} - \Pi_{ext} \tag{75}$$

$$\Pi_{int} = \Pi_{int}^m + \Pi_{int}^b + \Pi_{int}^{mb} + \Pi_{int}^s \tag{76}$$

$$\Pi_{ext} = \int_A w f_z dA \tag{77}$$

where f_z is the distributed load in the z direction, $\Pi_{int}^m, \Pi_{int}^b, \Pi_{int}^{mb}$ and Π_{int}^s are respectively, membrane, bending, coupled membrane-bending and shear strain energy. The latter is the main reason why we need the *Hu-Washizu* formulation to define the assumed shear strain which reads

$$\Pi_{int}^s = \frac{1}{2}\int_A <\underline{\gamma}>[H_s]\{\underline{\gamma}\}dA + \int_A <T>(\{\gamma\}-\{\underline{\gamma}\})dA \tag{78}$$

By computing the variation of Π_{int}^s with respect to T (shear force), we get the following orthogonality condition:

$$\int_A \langle\delta T\rangle(\{\gamma\}-\{\underline{\gamma}\})dA = 0 \tag{79}$$

This equation can be viewed as a constraint equation to be imposed on each element edge:

$$\int_0^{L_k} \delta T_{s_k}(\gamma_{s_k} - \underline{\gamma}_{s_k})ds = 0 \; ; k = 5,6,7,8 \qquad (80)$$

From (80) we can defined the kinematic relationships between the assumed shear strain $\underline{\gamma}_s$ as a constant on each sides and $\underline{\gamma}_{s_k}$ according to

$$\underline{\gamma}_{s_k} = \frac{1}{L_k}\int_0^{L_k} \gamma_{s_k}ds \; ; k = 5,6,7,8 \qquad (81)$$

where

$$\gamma_{s_k} = \underline{u}_{p_s}\cdot \underline{n}_k + \underline{\beta}\cdot \underline{t}_{s_k} \qquad (82)$$

By introducing (82) into (81), we have

$$\underline{\gamma}_{s_k} = \frac{1}{L_k}\int_0^{L_k} (\underline{u}_{p_s}\cdot \underline{n}_k + \underline{\beta}\cdot \underline{t}_{s_k})\,ds \qquad (83)$$

where $\underline{n}_k$ is the unit exterior normal vector on the corresponding side k of the element. On each side-k, we obtain those normal vectors by averaging the nodal values

$$\underline{n}_k = \frac{1}{2}(\underline{n}_i + \underline{n}_j) \qquad (84)$$

By introducing (68) into (83), we obtain

$$-\frac{2}{3}\phi_k\Delta\beta_{s_k} = \frac{1}{L_k}\int_0^{L_k} (\underline{u}_{p_s}\cdot \underline{n}_k + \underline{\beta}\cdot \underline{t}_{s_k})ds \qquad (85)$$

Moreover, from (44) to (49) we have

$$\underline{u}_{p_s} = \frac{1}{L_k}(\underline{u}_j - \underline{u}_i)$$
$$\underline{\beta}\cdot \underline{t}_{s_k} = \beta_s = \left(1-\frac{s}{L_k}\right)\beta_{s_i} + \frac{s}{L_k}\beta_{s_j} + 4\frac{s}{L_k}\left(1-\frac{s}{L_k}\right)\Delta\beta_{s_k} \qquad (86)$$

Finally, from (85) and (86), we have:

$$-\frac{2}{3}(1+\phi_k)\Delta\beta_{s_k} = \frac{1}{L_k} < n_{X_k} \quad n_{Y_k} \quad n_{Z_k} > \begin{Bmatrix} U_j - U_i \\ V_j - V_i \\ W_j - W_i \end{Bmatrix} +$$

$$\frac{1}{2} < \underline{t}_{s_k}\cdot R\underline{N}1_i \; \vdots \; \underline{t}_{s_k}\cdot R\underline{N}2_i \; \vdots \; \underline{t}_{s_k}\cdot R\underline{N}3_i > \begin{Bmatrix} \theta_{X_i} \\ \theta_{Y_i} \\ \theta_{Z_i} \end{Bmatrix} +$$

$$\frac{1}{2} < \underline{t}_{s_k}\cdot R\underline{N}1_j \; \vdots \; \underline{t}_{s_k}\cdot R\underline{N}2_j \; \vdots \; \underline{t}_{s_k}\cdot R\underline{N}3_j > \begin{Bmatrix} \theta_{X_j} \\ \theta_{Y_j} \\ \theta_{Z_j} \end{Bmatrix} \qquad (87)$$

With transformation in (87) applied on all four sides, the independent parameter $\{\Delta\beta_n\}$ becomes a function of degrees of freedom $\{u_n\}$; namely

$$\{\Delta\beta_n\} = [A_\Delta]^{-1}[A_u]\{u_n\} \qquad (88)$$

where:

$$[A_\Delta] = -\frac{2}{3}\begin{bmatrix} (1+\phi_5) & 0 & 0 & 0 \\ 0 & (1+\phi_6) & 0 & 0 \\ 0 & 0 & (1+\phi_7) & 0 \\ 0 & 0 & 0 & (1+\phi_8) \end{bmatrix} \qquad (89)$$

Substituting (88) into (56) we obtain the final expression of the curvature

$$\{\chi\} = [B_b(\xi,\eta)]\{u_n\}$$
$$[B_b(\xi,\eta)] = [B_{b_\beta}(\xi,\eta)] + [B_{b_{\Delta\beta}}(\xi,\eta)][A_\Delta]^{-1}[A_u] \qquad (90)$$

Substituting (88) into the expression of transversal shear strain deformation (74), we obtain:

$$\{\underline{\gamma}\} = [B_s(\xi,\eta)]\{u_n\}$$
$$[B_s(\xi,\eta)] = [B_{s_\gamma}(\xi,\eta)][A_{\phi\Delta}][A_u] \qquad (91)$$

where:

$$[A_{\phi\Delta}] = [A_\phi][A_\Delta]^{-1} = \begin{bmatrix} \frac{\phi_5}{(1+\phi_5)} & 0 & 0 & 0 \\ 0 & \frac{\phi_6}{(1+\phi_6)} & 0 & 0 \\ 0 & 0 & \frac{\phi_7}{(1+\phi_7)} & 0 \\ 0 & 0 & 0 & \frac{\phi_8}{(1+\phi_8)} \end{bmatrix} \qquad (92)$$

When $h \ll L_k$, it can easily be seen from the last result that ϕ_k becomes very small and consequently:

- Matrix $[A_\Delta]$ and bending energy for DKMQ24 will be equal with DKQ24 element in Ref. [62], therefore there is no shear locking for thin shell.
- Matrix $[A_{\phi\Delta}] \approx [0]$ and shear energy becomes zero, and the DKMQ24 element will converges to DKQ24 element in Ref. [62].

When $h \gg L_k$, it can easily be seen that ϕ_k becomes very large and consequently:

- Matrix $[A_\Delta]^{-1} \approx [0]$ and $\{\Delta\beta_n\} \approx \{0\}$; therefore, the bending strain matrix $[B_b]$ from (90) for DKMQ24 element will be almost identical to the bending strain matrix of Q4γ24 [11,52] element equivalent of MITC4 [27].
- Matrix $[A_{\phi\Delta}] \approx [I]$, therefore, the shear strain matrix $[B_s]$ defined in (91) for DKMQ24 element will be almost identical with the shear strain matrix for the Q4γ24 [11,52] element equivalent of MITC4 [27].
- For plates, DKMQ24 gives the same results as DKMQ [41] plate bending element and converges to MITC4 plate bending element [63].

For an element with the area A, the membrane strain energy (76) can be written as

$$\Pi_{int}^m = \frac{1}{2}\int_A \langle e \rangle [H_m]\{e\}dA = \frac{1}{2}\langle u_n \rangle [k_m]\{u_n\} \qquad (93)$$

where

$$[k_m] = \int_A [B_m]^T [H_m] [B_m]dA \qquad (94)$$

In a similar way, the bending deformation energy (76) for an element with the area A is given by

$$\Pi_{int}^b = \frac{1}{2}\int_A \langle \chi \rangle [H_b]\{\chi\}dA = \frac{1}{2}\langle u_n \rangle [k_b]\{u_n\} \qquad (95)$$

leading to the bending part of the proposed shell element stiffness

$$[k_b] = \int_A [B_b]^T [H_b][B_b]dA \qquad (96)$$

The membrane-bending coupling effects energy (76) for an element with the area A is given by

$$\Pi_{int}^{mb} = \frac{1}{2}\int_A \langle e \rangle [H_{mb}]\{\chi\}dA + \frac{1}{2}\int_A \langle \chi \rangle [H_{mb}]\{e\}dA$$
$$\Pi_{int}^{mb} = \frac{1}{2}\langle u_n \rangle ([k_{mb}] + [k_{mb}]^T)\{u_n\} \qquad (97)$$

leading to the coupling term of the shell element stiffness

$$[k_{mb}] = \int_A [B_m]^T [H_{mb}][B_b]dA \qquad (98)$$

Finally, transversal shear strain energy (76) for an element with the mid-surface area A is:

$$\Pi_{int}^s = \frac{1}{2}\int_A \langle \underline{\gamma} \rangle [H_s]\{\underline{\gamma}\}dA = \frac{1}{2}\langle u_n \rangle [k_s]\{u_n\} \qquad (99)$$

which allows us to define the shear term of the shell element stiffness matrix

$$[k_s] = \int_A [B_s]^T [H_s][B_s]\,dA \tag{100}$$

In summary, the stiffness matrix $[k]$ is the assembly of the stiffness matrices due to membrane, bending, coupled membrane-bending and transversal shear.

$$[k] = [k_m] + [k_b] + [k_{mb}] + [k_{mb}]^T + [k_s] \tag{101}$$

The stiffness matrix is determined using the Gauss numerical integration. The standard Gauss integration rule with 2×2 points is enough to integrate the stiffness matrix (94), (96), (98) and (100) with satisfying accuracy.

9. Fictitious stiffness and MacNeal stabilization

In the field of shell kinematic, there is no rotation around the normal axis (θ_z). Therefore the stiffness matrix $[k]$ (101) will contain the value zero at the slots for nodal variables θ_{zi}. As a result, it will arise four spurious modes in shell element stiffness matrix. If all elements are placed into a plane that results with all nodes coplanar, the stiffness matrix will have a spurious mode with respect to rotations around normal to the shell (so called drilling rotations [64]). Therefore, to avoid the difficulties dealing with spurious modes, we use a fictitious stiffness. With the addition of fictitious stiffness, three spurious modes will vanish, while the other spurious mode will be eliminated by *MacNeal* stabilization [52].

$$\Pi_{int} = \Pi_{int} + \Pi_{int}^{\theta_z} + \Pi_{int}^{\bar\theta_z} \tag{102}$$

We define a fictitious stiffness:

$$\Pi_{int}^{\theta_z} = \frac{1}{2}H_{LL}10^{-3}\int_A (\theta_{z,x}\theta_{z,x} + \theta_{z,y}\theta_{z,y})\,dA$$
$$\Pi_{int}^{\theta_z} = \frac{1}{2}\langle\theta_n\rangle[k_{\theta_z}]\{\theta_n\} \tag{103}$$

$$\theta_z(\xi,\eta) = \sum_{i=1}^4 N_i(\xi,\eta)\theta_{zi}$$

$$\theta_z(\xi,\eta) = \sum_{i=1}^4 N_i(\xi,\eta) < n_{X_i} \quad n_{Y_i} \quad n_{Z_i} > \begin{Bmatrix} \theta_{X_i} \\ \theta_{Y_i} \\ \theta_{Z_i} \end{Bmatrix} \tag{104}$$

where:

$$<\theta_n> = \{\theta_n\}^T = < \cdots \quad \theta_{X_i} \quad \theta_{Y_i} \quad \theta_{Z_i} \quad \cdots >_{i=1,4} \tag{105}$$

$$\begin{Bmatrix} \theta_{z,x} \\ \theta_{z,y} \end{Bmatrix} = [C^o]^T \begin{Bmatrix} \theta_{z,\xi} \\ \theta_{z,\eta} \end{Bmatrix} \tag{106}$$

Matrix $[k_{\theta_z}]_{12\times12}$ is expanded into matrix $[k_{\theta_z}]_{24\times24}$ to adjust the nodal variables in the element stiffness matrix.

We define a fictitious stiffness according to Mac Neal stabilization,

terms leading to:

$$\Pi_{int}^{\bar\theta_z} = \frac{1}{2}G_{LT}10^{-3}\int_A (\bar\theta_z\cdot\bar\theta_z)\,dA = \frac{1}{2}\langle u_n\rangle[k_{\bar\theta_z}]\{u_n\} \tag{107}$$

where we used a small arbitrary factor of stabilization of 10^{-3} that will not affect the results but will enable to avoid singularities. The final form of the stiffness matrix is:

$$[\bar k] = [k] + [k_{\theta_z}] + [k_{\bar\theta_z}] \tag{108}$$

In this format, it is important to notice that matrix $[k_{\bar\theta_z}]_{12\times12}$ is expanded into matrix $[k_{\bar\theta_z}]_{24\times24}$ to adjust the nodal variables in the element stiffness matrix. Therefore, the rank of matrix $[k_{\theta_z}]$ is three and rank of matrix $[k_{\bar\theta_z}]$ is one. The addition of small fictitious stiffness $[k_{\theta_z}]$ and $[k_{\bar\theta_z}]$ will not affect the precision and the rate of convergence. Matrix $[k_{\theta_z}]$ eliminates the numerical singularity in the element when the four nodes are coplanar. Finally, the DKMQ24 element has rank = 18, with 6 rigid body modes without any spurious mode and without any spurious constraint when the four nodes are coplanar.

10. Numerical simulations

To validate our new DKMQ24 shell element for composite structures, we will use the tests proposed by Srinivas [65] and Pagano and Hatfield [66,67] for plate problems. Moreover, for composite shell problems we consider the test proposed by Varadan and Bhaskar [68], along with a new hyperbolic paraboloid shell test.

The convergence of finite element formulation generally is measured by using the displacements or stresses at one point of the structures as a function of mesh refinement. But is better to consider, the method called *s-norm,* proposed in [69,70] will be used to get the behavior of the whole structure and to evaluate uniform and optimal convergence. The *s-norm,* defined in [69,70], is briefly presented in the Appendix A.

10.1. Simply supported (SS) under uniform loading of a sandwich plate

For the first test to validate our new element, we will use the test proposed by Srinivas [65]. Fig. 11 shows the details of this test in terms of chosen geometric and material properties. We will only analyze one quarter with area *ABCD*. The layer 2 (core) properties are proportional to those of layers 1 and 3, where *E* and *G* values of the core are *C* times weaker than those of the skin (*C* = 1, *C* = 10, and *C* = 50 are evaluated in this test).

Table 2 reports the results of central deflection at point *C* for $L/h = 10$, where the analytical computation result based on 3D elasticity theory [65] is used as the reference solution. The central displacement of point *C* is expressed in the form:
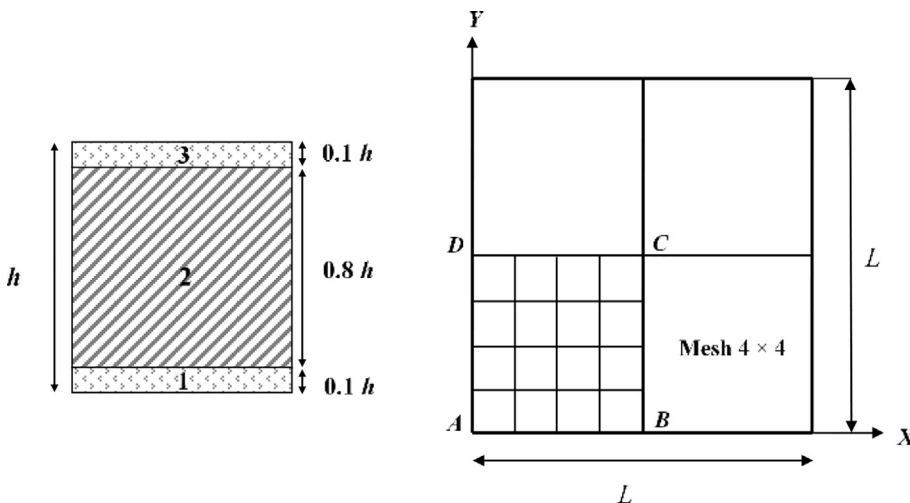

Fig. 11. Simply supported square sandwich plate under uniform loading. Data material (skin and core orthotropic): $E_L = 3.4156$ MPa; $E_T = 1.7931$ MPa; $\upsilon_{LT} = 0.44$; $G_{LT} = 1$ MPa; $G_{LZ} = 0.608$ MPa; $G_{TZ} = 1.015$ MPa; Stratification: sandwich; 3-layered 0/0/0 symmetrical; $L = 1000$; $h = 100$. Boundary Conditions: $W = \theta_Y = 0$ along *AB* and $W = \theta_X = 0$ along *AD*. Symmetrical conditions: $U = \theta_Y = 0$ along *BC*, $V = \theta_X = 0$ along *DC*.

Table 2
Convergence of central deflection $\underline{W}_C$ ($L/h = 10$) with uniform mesh.

$N \times N$	$C = 1$ $\kappa_{11} = \kappa_{22} = 0.8333$; $\kappa_{12} = 0$		$C = 10$ $\kappa_{11} = \kappa_{22} = 0.3521$; $\kappa_{12} = 0$		$C = 50$ $\kappa_{11} = \kappa_{22} = 0.0938$; $\kappa_{12} = 0$	
	DKMQ24	MITC4	DKMQ24	MITC4	DKMQ24	MITC4
4×4	180.621	180.690	41.912	41.982	16.902	16.921
8×8	181.115	181.190	41.973	41.994	16.854	16.858
16×16	181.290	181.310	41.992	41.997	16.842	16.843
32×32	181.339	181.350	41.996	41.998	16.839	16.839
64×64	181.351	181.350	41.998	41.998	16.838	16.838
Srinivas [65]	181.050		41.906		16.753	

Table 3
Convergence of central deflection $\underline{W}_C$ ($L/h = 10$) computed with distorted mesh.

| $N \times N$	$C = 1$ $\kappa_{11} = \kappa_{22} = 0.8333$; $\kappa_{12} = 0$		$C = 10$ $\kappa_{11} = \kappa_{22} = 0.3521$; $\kappa_{12} = 0$		$C = 50$ $\kappa_{11} = \kappa_{22} = 0.0938$; $\kappa_{12} = 0$	
	DKMQ24	MITC4	DKMQ24	MITC4	DKMQ24	MITC4
4×4	182.776	183.616	42.269	42.591	17.028	17.104
8×8	181.515	181.905	42.052	42.143	16.884	16.903
16×16	181.374	181.492	42.011	42.034	16.849	16.854
32×32	181.358	181.389	42.001	42.007	16.841	16.842
64×64	181.356	181.364	41.999	42.000	16.838	16.839
Ref. [65]	181.050		41.906		16.753	

$$\underline{W}_C = \frac{W_C \, G_{LT} \, (\text{Core})}{h f_z}$$

All numerical results obtained are very close to the reference solution. We have also checked that DKMQ24 and MITC4 [27] give similar results.

To get the behavior of the whole structure, the *s-norm* test is performed. Figs. 12 and 13 present the convergence behavior of DKMQ24 and MITC4 [27] elements in composite application using $L/h = 4$, 10,

100, 1000 and 10,000. The result of DKMQ24 with $N \times N = 128 \times 128$ is used as reference solution. We found that the result of DKMQ24 element are similar to MITC4 for thick plate problem. However, in thin plate problem, DKMQ24 element leads to smaller errors.

To study the sensitivity of the DKMQ24 element, we analyze the same test using distorted meshes presented in Fig. 14. The central deflection at point C for $L/h = 10$ compared to the reference values of Srinivas [65] is presented in Table 3. The two elements give the results
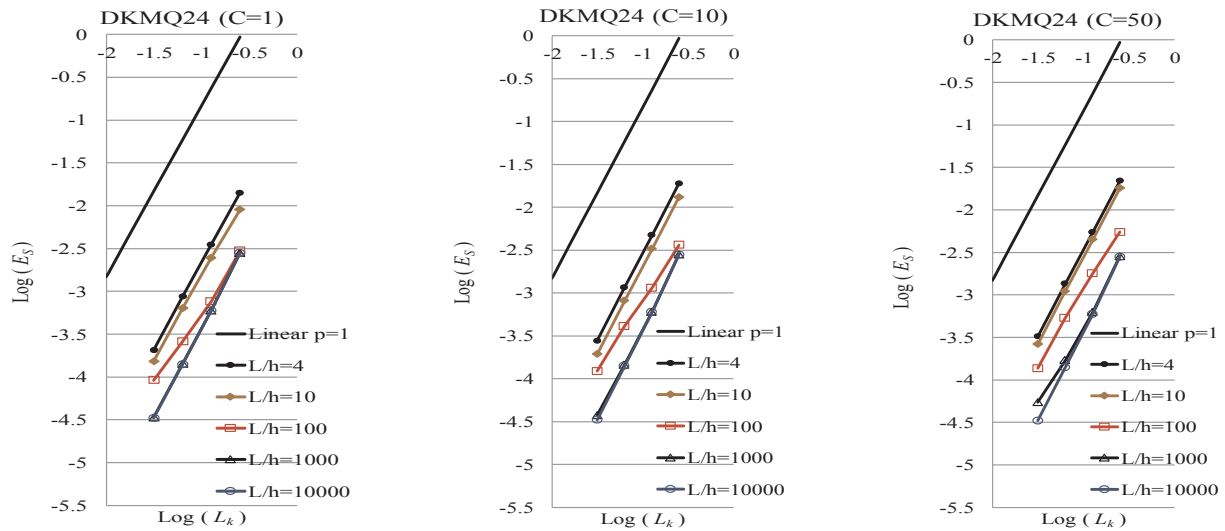
Fig. 12. Convergence behavior of SS sandwich square plate by using *s-norm* for DKMQ24 element (regular mesh).
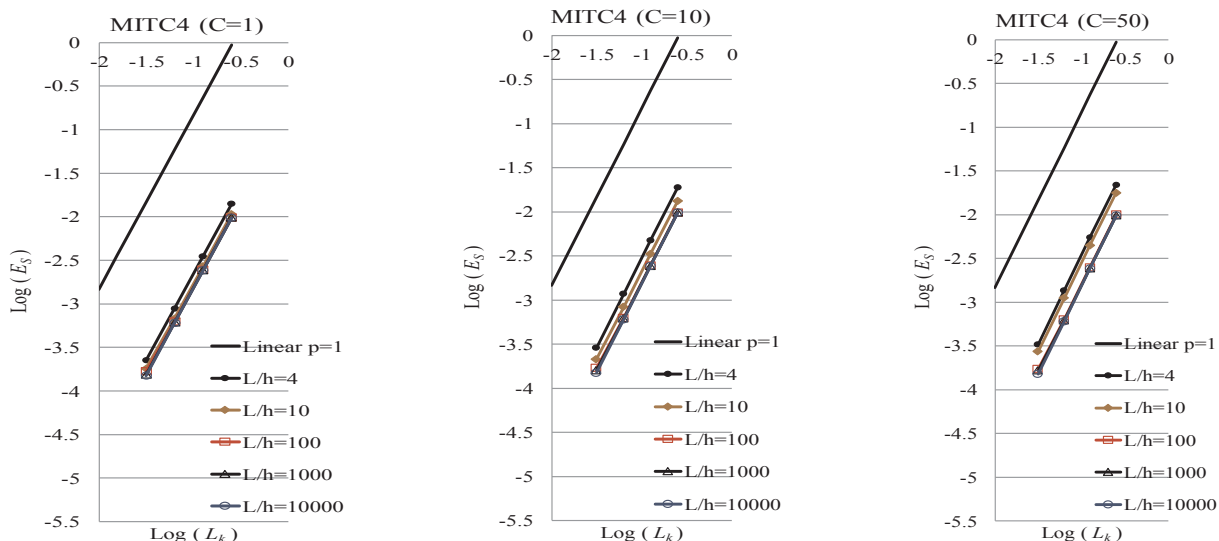
Fig. 13. Convergence behavior of SS sandwich square plate by using *s-norm* for MITC4 (regular mesh).
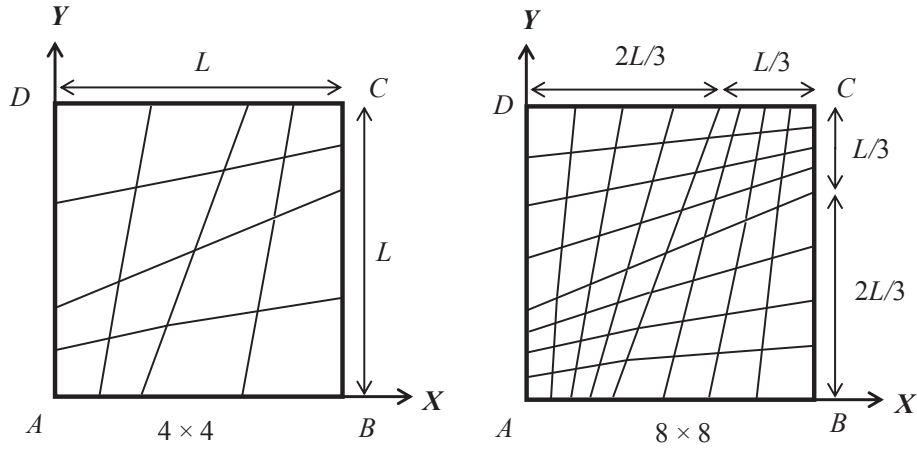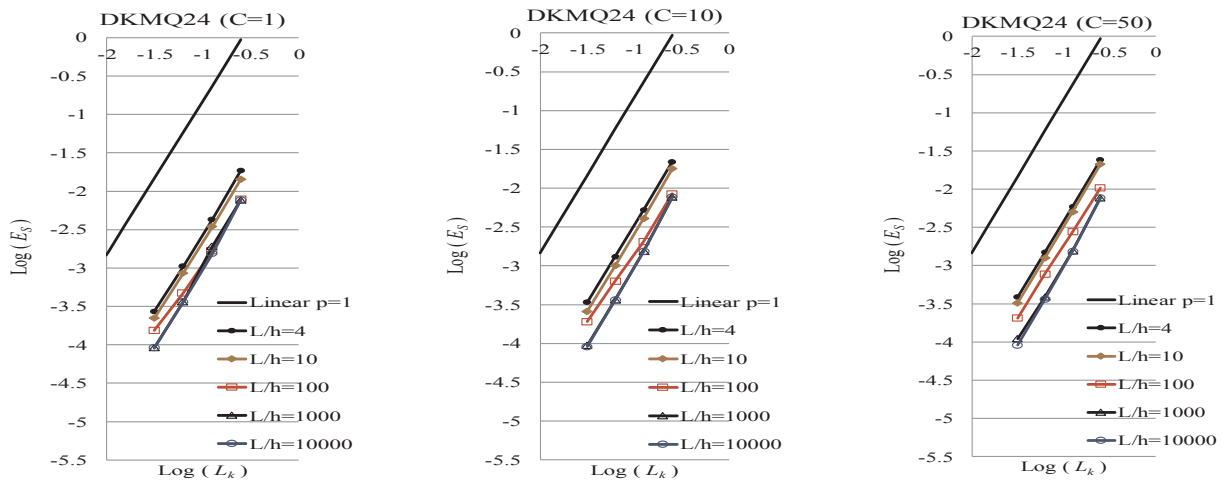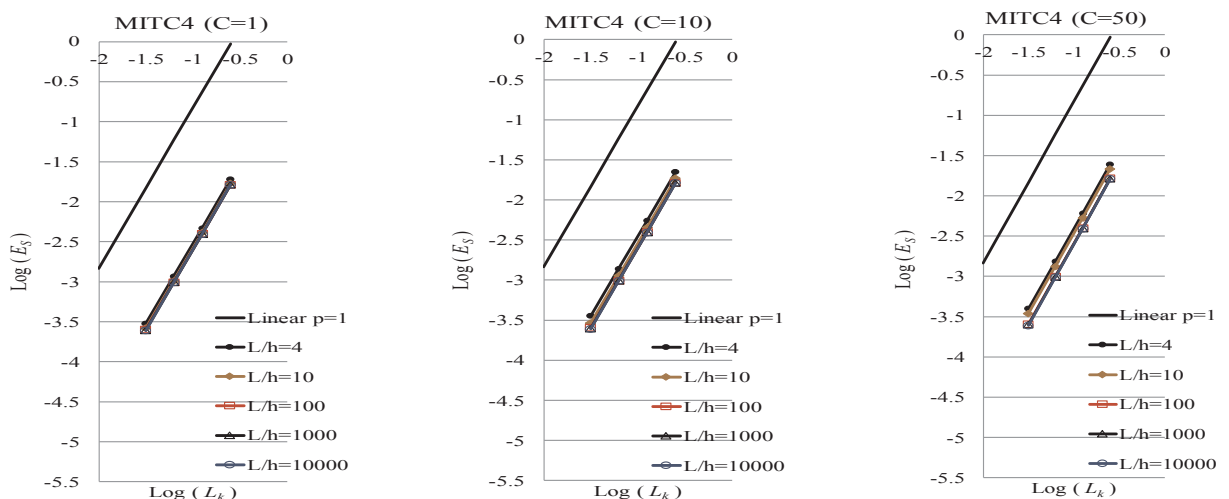
Fig. 14. Distorted mesh of square plate.

Fig. 15. Convergence behavior of SS sandwich square plate by using *s-norm* for DKMQ24 (distorted mesh).

that converge to the reference solution for all value of *C*. Figs. 15 and 16 present the convergence behavior of DKMQ24 and MITC4 [27] elements by using the distorted mesh. We found that the behavior of DKMQ24 is similar to the MITC4 element for thick plate problem. Moreover, this test reveals that DKMQ24 and MITC4 elements in composite application are not very sensitive to mesh distortion.

10.2. Non-symmetric sandwich plate

We analyze simply supported square sandwich plate with non-symmetric layer arrangement under uniform loading f_z. For the plate section non-symmetry, there is a coupling between bending and membrane effects. We can see the data for this test in Fig. 17. Because of symmetry, in the loading and boundary conditions, we only analyze one quarter with

Fig. 16. Convergence behavior of SS sandwich square plate by using *s-norm* for MITC4 (distorted mesh).
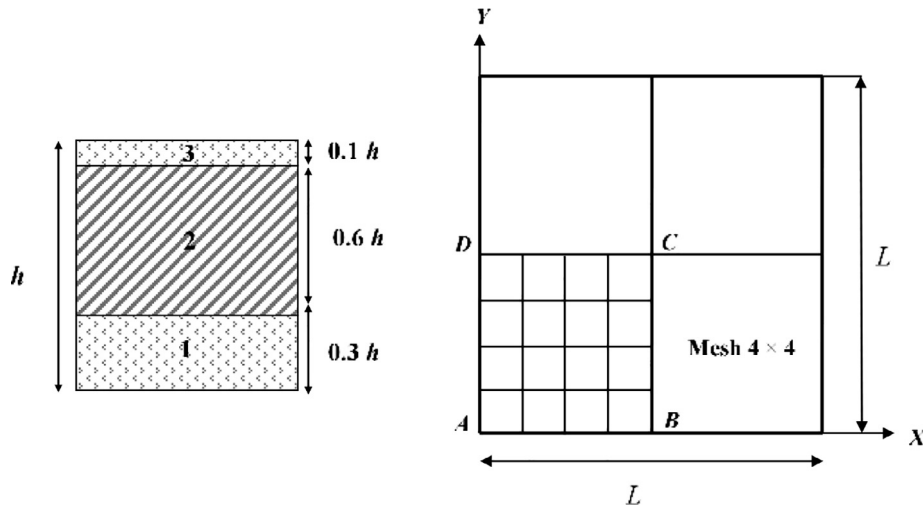
Fig. 17. Simply supported square sandwich plate non-symmetry. Data material (skin and core orthotropic): $E_L = 3.4156$ MPa; $E_T = 1.7931$ MPa; $\upsilon_{LT} = 0.44$; $G_{LT} = 1$ MPa; $G_{LZ} = 0.608$ MPa; $G_{TZ} = 1.015$ MPa. Boundary Conditions: $W = \theta_Y = 0$ along AB and $W = \theta_X = 0$ along AD. Symmetrical conditions: $U = \theta_Y = 0$ along BC, $V = \theta_X = 0$ along DC.

Table 4
Convergence of central deflection $\underline{W}_C$ of simply supported square sandwich plate non-symmetry.

$N \times N$	$\kappa_{11} = \kappa_{22} = 0.2449;\ \kappa_{12} = 0$	
	DKMQ24	MITC4
4×4	34.686	34.740
8×8	34.728	34.744
16×16	34.740	34.744
32×32	34.743	34.744
64×64	34.744	34.745
Ref. [65]	34.549	

area ABCD. The layer 2 (core) properties are proportional to those of layers 1 and 3, where E and G values of the core are 10 times weaker than those of the skin. We check the convergence of numerical results computed by DKMQ24 against the reference solution by Srinivas [65].

We can validate our element DKMQ24 by comparing the vertical displacement in point C against the reference solution by Srinivas [65] and also provide a comparison to the other element. The reference of central displacement is given by

$$\underline{W}_C = \frac{W_C\, G_{LT}\,(\text{Core})}{h f_z}$$

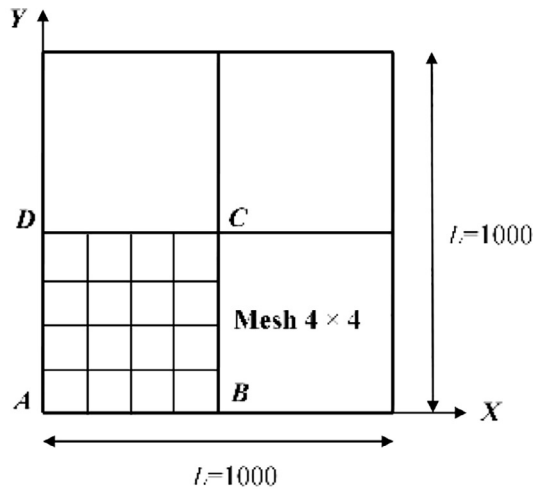The central deflection at point C for $L/h = 10$ compared to the

Fig. 18. Simply supported 3-layered and 9-layered square plates. Material properties: $E_L = 25$ MPa; $E_T = 1$ MPa; $\upsilon_{LT} = \upsilon_{TZ} = 0.25$; $G_{LT} = 0.5$ MPa; $G_{TZ} = 0.2$ MPa; $f_z = f_0$ $\sin(\pi x/L)$ $\sin(\pi y/L)$; for 3-*layered*: $\kappa_{11} = 0.570$; $\kappa_{22} = 0.882$; $\kappa_{12} = \kappa_{21} = 0$; 0/90/0 symmetrical; for 9-*layered*: $\kappa_{11} = 0.670$; $\kappa_{22} = 0.666$; $\kappa_{12} = \kappa_{21} = 0$; 0/90/0/90/0/90/0/90/0 symmetrical. Boundary Conditions: $W = \theta_Y = 0$ along AB and $W = \theta_X = 0$ along AD. Symmetrical conditions: $U = \theta_Y = 0$ along BC, $V = \theta_X = 0$ along DC.
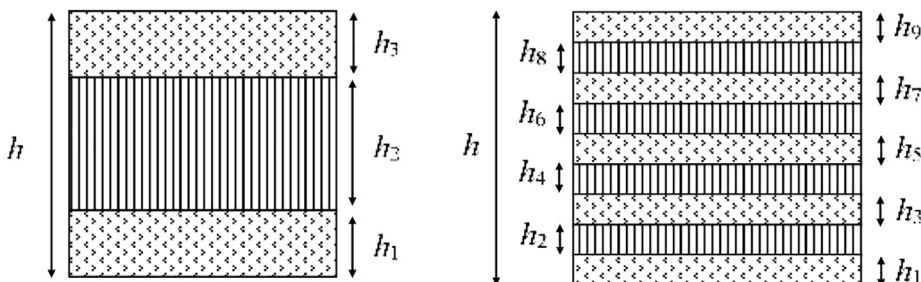
Table 5
Convergence of central deflection $\underline{W}_C$ of simply supported 3-layered square plate.

$N \times N$	3-layered							
	$L/h = 4$		$L/h = 10$		$L/h = 50$		$L/h = 100$	
	DKMQ24	MITC4	DKMQ24	MITC4	DKMQ24	MITC4	DKMQ24	MITC4
4×4	4.785	4.768	1.746	1.734	1.030	1.018	1.005	0.993
8×8	4.755	4.751	1.740	1.737	1.030	1.027	1.005	1.003
16×16	4.748	4.747	1.738	1.738	1.030	1.029	1.006	1.005
32×32	4.746	4.746	1.738	1.738	1.030	1.029	1.006	1.005
64×64	4.745	4.745	1.738	1.738	1.030	1.030	1.006	1.006
Ref. [66,67]	4.491		1.709		1.031		1.008	

Table 6
Convergence of central deflection $\underline{W}_C$ of simply supported 9-layered square plate.

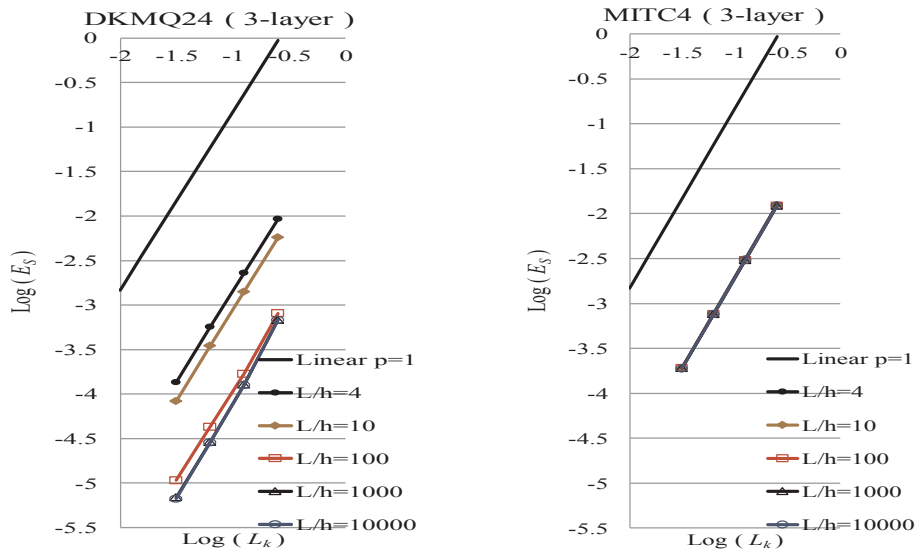| $N \times N$	9-layered							
	$L/h = 4$		$L/h = 10$		$L/h = 50$		$L/h = 100$	
	DKMQ24	MITC4	DKMQ24	MITC4	DKMQ24	MITC4	DKMQ24	MITC4
4×4	4.200	4.188	1.517	1.505	1.018	1.006	1.002	0.990
8×8	4.170	4.167	1.512	1.509	1.018	1.015	1.003	1.000
16×16	4.162	4.161	1.511	1.511	1.018	1.017	1.003	1.002
32×32	4.160	4.160	1.511	1.511	1.018	1.018	1.003	1.002
64×64	4.160	4.160	1.511	1.511	1.018	1.018	1.003	1.003
Ref. [66,67]	4.079		1.512		1.021		1.005	

Fig. 19. Convergence behavior of 3-layered square plate by using *s-norm* with uniform mesh.

reference values of Srinivas [65] is presented in Table 4. All the numerical results obtained are very close to the reference solution. We have also checked that DKMQ24 and MITC4 [27] give similar results.

10.3. Simply supported 3-layered and 9-layered square plate under sinusoidal pressure load

In this test, we analyze a simply supported 3-layered and 9-layered unidirectional square laminated, composite plate with $L = 1000$ and different thickness, using DKMQ24 shell element. We carry out the analysis for uniform and distorted mesh, and compare the performance of DKMQ24 element against MITC4 [27] element. This test is proposed by Pagano and Hatfield [66,67], with the details presented in Fig. 18.

The solution for vertical displacement in point C is expressed with the following form:

$$\underline{W}_C = \frac{\pi^4 W_C Q}{12 S^4 h f_o}$$

$$S = \frac{L}{h} \; ; \; Q = 4G_{LT} + \frac{(E_L + E_T(1 + 2\upsilon_{TZ}))}{(1 - \upsilon_{LT}\upsilon_{TZ})}$$

We can see in Tables 5 and 6 the computed central displacement for 3-layered and 9-layered matches very well the reference solution given by Pagano and Hatfield [66,67] when using uniform mesh. We also found a good agreement between DKMQ24 and MITC4 [27] elements. Figs. 19 and 20 show the convergence behavior of DKMQ24 and MITC4 elements in composite application. When using $L/h = 4$, 10, 100, 1000 and 10,000 and results of DKMQ24 with $N \times N = 128 \times 128$ as the reference solution, we find again that DKMQ24 element has similar behavior with MITC4 element for thick plate problem. On the contrary, in thin plate problem, DKMQ24 element gives smaller error than MITC4 element.

Tables 7 and 8 present the central displacement for 3-layered and 9-layered compared with the reference solution given by Pagano and Hatfield [66,67] using distorted mesh shown in Fig. 14. We found a good
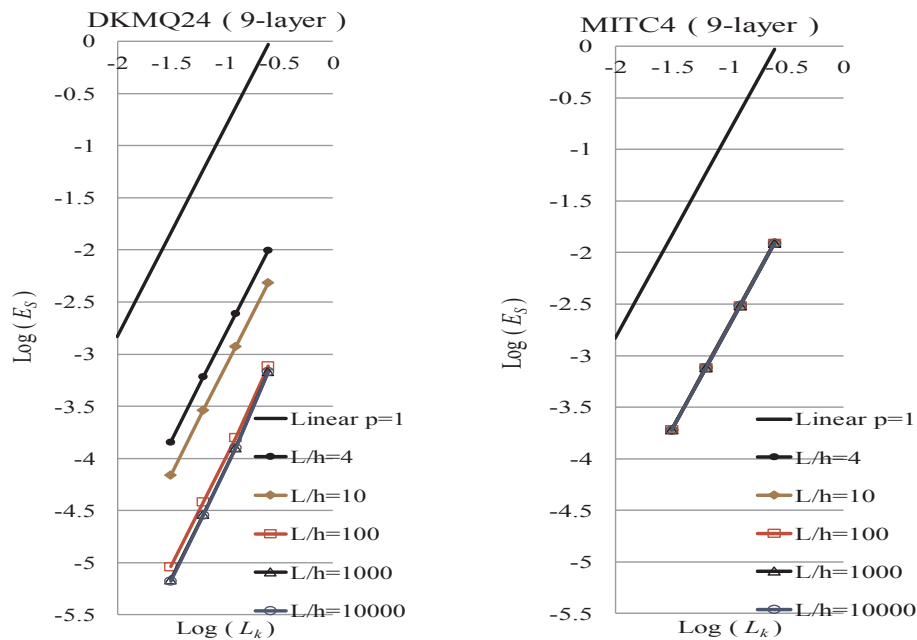
Fig. 20. Convergence behavior of 9-layered square plate by using *s-norm* with uniform mesh.

Table 7
Convergence of central deflection $\underline{W}_C$ of simply supported 3-layered square plate (distorted mesh).

$N \times N$	3-layered							
	$L/h = 4$		$L/h = 10$		$L/h = 50$		$L/h = 100$	
	DKMQ24	MITC4	DKMQ24	MITC4	DKMQ24	MITC4	DKMQ24	MITC4
4×4	4.804	4.789	1.751	1.750	1.043	1.030	1.022	1.005
8×8	4.760	4.756	1.741	1.741	1.031	1.030	1.009	1.005
16×16	4.749	4.748	1.739	1.739	1.030	1.030	1.006	1.005
32×32	4.746	4.746	1.738	1.738	1.030	1.030	1.006	1.006
64×64	4.746	4.745	1.738	1.738	1.030	1.030	1.006	1.006
Ref. [66,67]	4.491		1.709		1.031		1.008	

Table 8
Convergence of central deflection $\underline{W}_C$ of simply supported 9-layered square plate (distorted mesh).

$N \times N$	9-layered							
	$L/h = 4$		$L/h = 10$		$L/h = 50$		$L/h = 100$	
	DKMQ24	MITC4	DKMQ24	MITC4	DKMQ24	MITC4	DKMQ24	MITC4
4×4	4.216	4.201	1.529	1.515	1.029	1.015	1.014	0.999
8×8	4.174	4.167	1.515	1.512	1.021	1.017	1.005	1.002
16×16	4.163	4.162	1.512	1.511	1.019	1.018	1.003	1.002
32×32	4.160	4.160	1.511	1.511	1.018	1.018	1.003	1.003
64×64	4.160	4.160	1.511	1.511	1.018	1.018	1.003	1.003
Ref. [66,67]	4.079		1.512		1.021		1.005	

correlation between the numerical results computed both by DKMQ24 and MITC [27] elements with the reference solution. Figs. 21 and 22 show the convergence behavior of DKMQ24 and MITC4 [27] elements in composite plate application by using *s-norm*. For uniform mesh, $L/h = 4$, 10, 100, 1000 and 10,000 and the results of DKMQ24 with $N \times N = 128 \times 128$ taken as reference solution, we found again that DKMQ24 element has similar behavior with MITC4 element in thick plate problem. Moreover, the two elements are not sensitive to the mesh distortion.

10.4. Three-layered cylindrical shell with sinusoidal pressure

In this test, we will analyze a three-layered cylindrical shell with

sinusoidal pressure. Because of symmetry, we will analyze only one quarter of the shell, with the area *ABCD* shown in Fig. 23. This test was first analyzed by Ren [71], providing an analytical solution, which was then revisited by Varadan et Bhaskar [68] who proposed a solution based on 3D elasticity.

We compare the vertical displacement at point *C* with the reference solution in [68]. Table 9 shows the comparison of DKMQ24 and MITC4 elements with reference solution for different ratios of *R/h*. The reference value of central displacement is given by [68]:

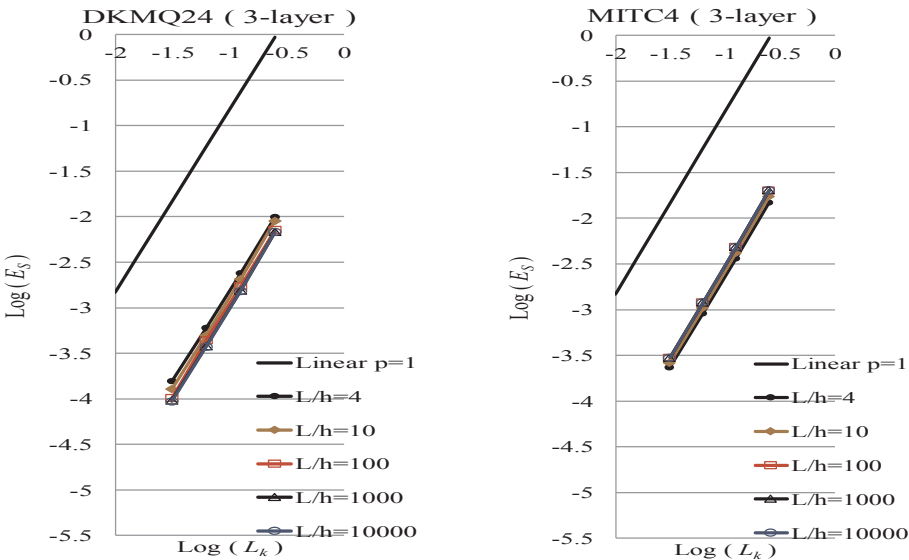$$\underline{W}_C = \frac{10 E_L}{f_0 S^4 h} W_C \; ; S = \left(\frac{R}{h} \right)$$

Fig. 21. Convergence behavior of 3-layered square plate by using *s-norm* (distorted mesh).
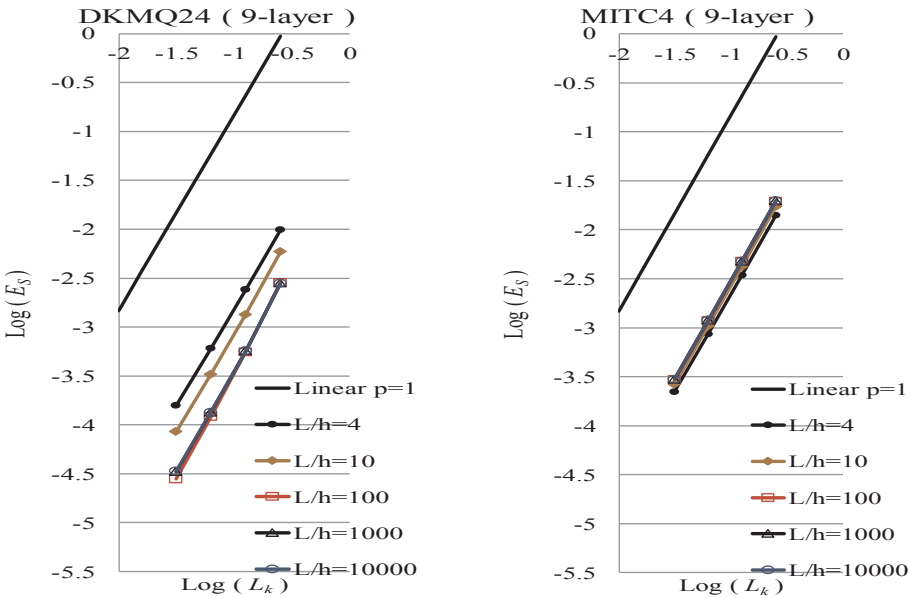

Fig. 22. Convergence behavior of 9-layered square plate by using *s-norm* (distorted mesh).
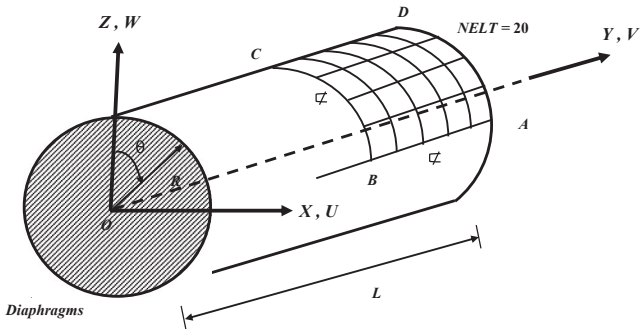

Fig. 23. Three-layered cylindrical shell. Internal sinusoidal loading $Q = f_0 \sin(\pi Y/L) \cos(4\theta)$; 3-layered 90/0/90; $L = 80$ m; $R = 20$ m; $E_L = 25$ MPa; $E_T = 1$ MPa; $\upsilon_{LT} = 0.25$; $G_{LT} = 0.5$ MPa; $G_{TZ} = 0.2$ MPa; Boundary condition: $U = W = \theta_Y = 0$ on the side AD; Symmetry conditions: $W = \theta_Y = \theta_X = 0$ on the side AB; $V = \theta_X = \theta_Z = 0$ on the side BC; $U = \theta_Y = \theta_Z = 0$ on the side CD.

Table 9
Convergence of central deflection $\underline{W}_C$ of three-layered cylindrical shell with sinusoidal pressure.

NELT	$R/h = 50$		$R/h = 100$		$R/h = 500$	
	DKMQ24	MITC4	DKMQ24	MITC4	DKMQ24	MITC4
4 × 5 = 20	0.4411	0.3411	0.3766	0.2957	0.0779	0.0736
8 × 10 = 80	0.5156	0.4909	0.4447	0.4247	0.0960	0.0950
16 × 20 = 320	0.5380	0.5319	0.4647	0.4598	0.1011	0.1008
32 × 40 = 1280	0.5439	0.5423	0.4700	0.4687	0.1023	0.1023
64 × 80 = 5120	0.5464	0.5461	0.4714	0.4611	0.1026	0.1026
Ref. [68]	0.5495		0.4715		0.1027	

By using NELT = 20, 80, 320, 1280 and 5120 (NELT = 20 shows in Fig. 23) and $R/h = 50$, 100 and 500, the vertical displacement of point C are presented in Fig. 24 and Table 9. The two elements give very good results compared to the reference solution. We can see that DKMQ24 element converges faster than MITC4 [27] element.
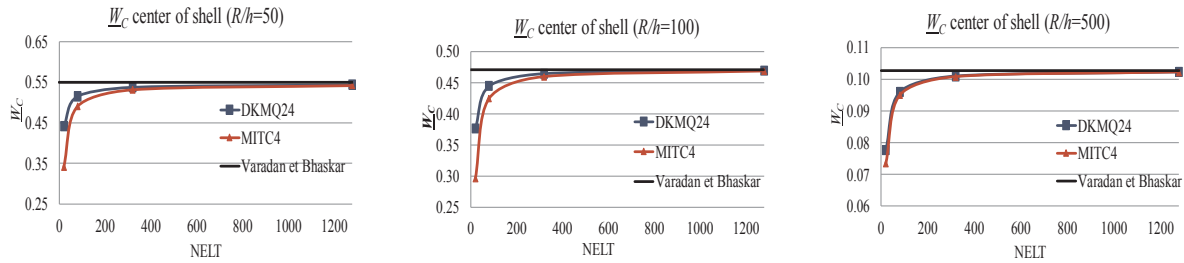
Fig. 24. Convergence of central deflection $\underline{W}_C$ of 3-layered cylindrical shell with sinusoidal pressure.
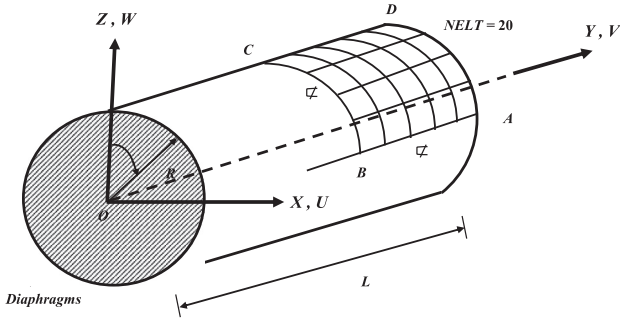

Fig. 25. Ten-layered cylindrical shell. Internal sinusoidal loading Q = f_0 sin(πY/L) cos (4θ); L = 80 m; R = 20 m; 10-layered $(90/0/90/0/90)_S$; E_L = 25 MPa; E_T = 1 MPa; υ_{LT} = 0.25; G_{LT} = 0.5 MPa; G_{TZ} = 0.2 MPa; Boundary condition: U = W = θ_Y = 0 on the side AD; Symmetry conditions: W = θ_Y = θ_X = 0 on the side AB; V = θ_X = θ_Z = 0 on the side BC; U = θ_Y = θ_Z = 0 on the side CD.

Fig. 27. Hyperbolic paraboloid shells. *Data*: a = 50 cm; b = 10 cm; h = 0.8 cm; distributed load in the normal direction: f_z = 0.01 kg/cm^2; Z = (b/a^2) XY; Boundary conditions: U = V = W = θ_X = θ_Y = θ_Z = 0 along sides ABCD; E_L = 3.4156 MPa; E_T = 1.7931 MPa; υ_{LT} = 0.44; G_{LT} = 1 MPa; G_{LZ} = 0.608 MPa; G_{TZ} = 1.015 MPa; Stratification: 3-layered 0/0/0 symmetrical.

central displacement is given by [68]:

$$\underline{W}_C = \frac{10E_L}{f_0 S^4 h}W_C \; ; S = \left(\frac{R}{h}\right)$$

Similarly, to the previous test, we use NELT = 20, 80, 320, 1280 and 5120 (NELT = 20 shows in Fig. 25) and R/h = 50, 100 and 500. The computed numerical results for vertical displacement at point C are presented in Fig. 26 and Table 10. The two elements give very good results converging to the reference solution. We can see that DKMQ24 element converges faster than MITC4 element.

Table 10
Convergence of central deflection $\underline{W}_C$ of simply supported 10-layered cylindrical shell.

NELT	R/h = 50		R/h = 100		R/h = 500	
	DKMQ24	MITC4	DKMQ24	MITC4	DKMQ24	MITC4
4 × 5 = 20	0.6178	0.4778	0.4983	0.3983	0.0755	0.0721
8 × 10 = 80	0.7235	0.6885	0.5917	0.5669	0.0938	0.0927
16 × 20 = 320	0.7548	0.7461	0.6188	0.6126	0.0989	0.0983
32 × 40 = 1280	0.7629	0.7607	0.6258	0.6242	0.1002	0.0997
64 × 80 = 5120	0.7678	0.7673	0.6274	0.6271	0.1005	0.0992
Ref. [68]	0.7622		0.6261		0.1006	

10.5. Ten-layered cylindrical shell with sinusoidal pressure

In this test, we will analyze ten-layered cylindrical shell loaded with sinusoidal pressure. Because of symmetry, we will analyze only the area ABCD in the Fig. 25. This test has been studied by Ren [71] analytical solution, then revisited by Varadan et Bhaskar [68] who proposed a reference solution based on 3D elasticity.

We compare the vertical displacement of point C with the reference solution in [68]. In Table 10, which shows the comparison of numerical results obtained with DKMQ24 and MITC4 [27] elements against the reference solution for different ratio of R/h. The reference value of
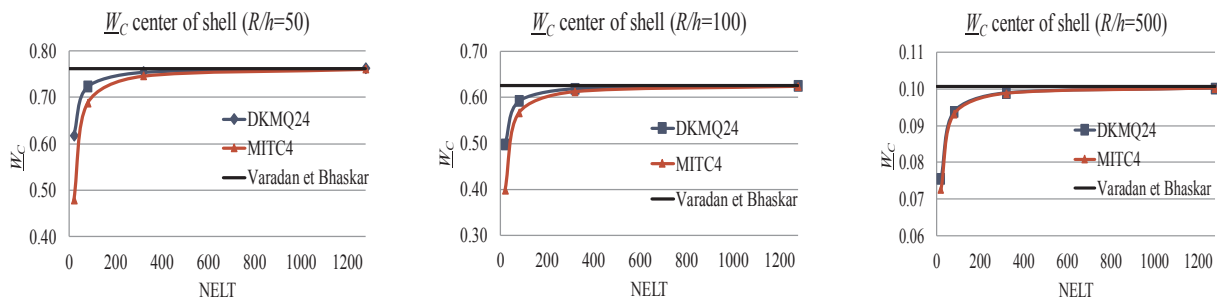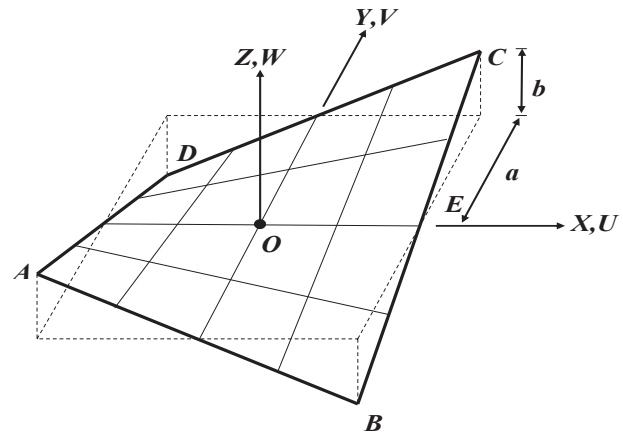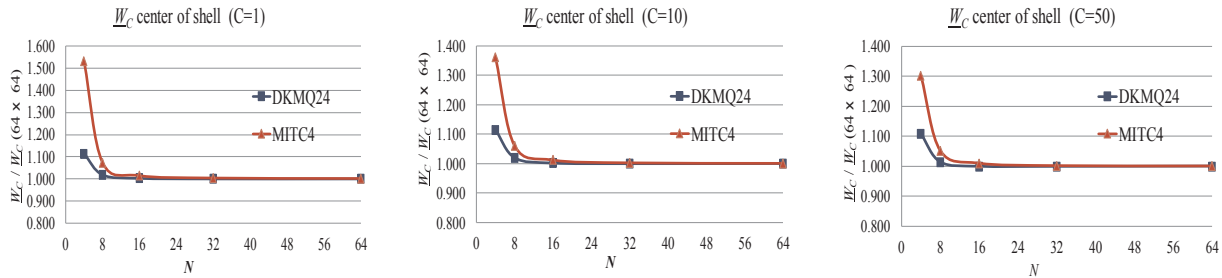
10.6. Hyperbolic paraboloid shells

Another problem is the problem of a hyperbolic paraboloid composite shell with a distributed load in the normal direction f_z. Fig. 27 presents the geometry and mechanical characteristic of this problem.

This particular shell has a negative Gaussian curvature with boundary conditions along the straight lines. The projection is a rectangular-shape, with bases 2a × 2a, and clamped on the sides. This

Fig. 26. Convergence of central deflection $\underline{W}_C$ of 10-layered cylindrical shell with sinusoidal pressure.

Table 11
Convergence of central deflection $\underline{W}_C$ ($L/h = 100$) of hyperbolic paraboloid shells.

$N \times N$	$C = 1$ $\kappa_{11} = \kappa_{22} = 0.8333; \kappa_{12} = 0$		$C = 10$ $\kappa_{11} = \kappa_{22} = 0.3521; \kappa_{12} = 0$		$C = 50$ $\kappa_{11} = \kappa_{22} = 0.0938; \kappa_{12} = 0$	
	DKMQ24	MITC4	DKMQ24	MITC4	DKMQ24	MITC4
4×4	34.001	46.742	124.060	151.447	156.532	183.863
8×8	31.093	32.755	113.448	117.973	143.202	148.531
16×16	30.068	30.952	111.451	112.619	141.148	142.667
32×32	30.530	30.500	110.212	111.569	141.104	141.540
64×64	30.529	30.555	111.279	111.382	141.253	141.373

Fig. 28. Convergence of central deflection $\underline{W}_C / W_C$ (DKMQ24 with mesh 64 × 64) of hyperbolic paraboloid shells.

shell geometry corresponds to a shallow shell.

The layer 2 (core) properties are proportional to those of layers 1 and 3, where E and G values of the core are C times weaker than those of the skin ($C = 1$, $C = 10$, and $C = 50$ are evaluated in this test). Table 11 and Fig. 28 present the convergence of the deflection $\underline{W}_C = W_C \times 10^3$ versus the number of elements. We can see that DKMQ24 and MITC4 [27] gives good results.

11. Conclusions

The new four nodes and 24 *dof* quadrilateral shell element DKMQ24, using incomplete quadratic interpolation functions for the rotations, has been presented and evaluated for thick and thin shell composite problems. The presents DKMQ24 element is valid for any-shell principal curvatures and position on the four nodes on the middle surface due to proper coupling between membrane and bending displacement to define the bending strain [11,52]. DKMQ24 element can equally reproduce the behavior in accordance with the theory of *Kirchhoff* and *Reissner-Mindlin*, due to the use of a shear influence factor

ϕ_k which is a function of shell thickness ratio.

This also explains the position of the DKMQ24 element relative to the MITC4 [27] and DKQ24 [62] shell elements. The DKMQ24 element will become identical to the MITC4 element when ϕ_k is very large. On the other hand, the DKMQ24 element become identical to the DKQ24 [62] element when ϕ_k is very small.

The results of the analysis show that this element can pass all standard convergence tests, without membrane locking. It is also free of shear locking, as the DKMQ plate element [41]. In bending dominated problems, results obtained with DKMQ24 element are very good and the convergence is faster than with MITC4. This is due to the quadratic interpolation functions for the rotations used in DKMQ24.

Acknowledgments

Appendix A

A.1. S-NORM METHOD

Uniform and optimal convergence of elements can be assessed using *s-norm* tests as defined in [72,73,70,74].

The relative error is computed using the general expression:

$$E_S = \frac{||e^{FE}||^2}{||\Pi_{int}^{Ref}||^2} = \frac{||\Pi_{int}^{Ref} - \Pi_{int}^{FE}||^2}{||\Pi_{int}^{Ref}||^2} \tag{A-1}$$

where: $||\Pi_{int}^{Ref}||^2$ refers to the strain energy of the reference solution which can be defined by an analytical expression or numerically by using a very fine mesh with "good" elements.

Even if an analytical solution is available it is not always easy to express $||\Pi_{int}^{Ref}||^2$ and usually a very fine mesh is used.

For the present plate bending problems, we then have:

$$||\Pi_{int}^{Ref}||^2 = \sum_{1}^{NELT} ||\Pi_{int}^{Ref}||_e^2 \tag{A-2}$$

NELT is the total number of elements in the reference mesh.

$$||\Pi_{int}^{Ref}||_e^2 = \frac{1}{2} \int_A \langle N_{Ref} \rangle [H_m]^{-1} \{N_{Ref}\} dA +$$

$$\frac{1}{2} \int_A \langle M_{Ref} \rangle [H_b]^{-1} \{M_{Ref}\} dA +$$

$$\frac{1}{2} \int_A \langle N_{Ref} \rangle [H_{mb}]^{-1} \{M_{Ref}\} dA +$$

$$\frac{1}{2} \int_A \langle M_{Ref} \rangle [H_{mb}]^{-1} \{N_{Ref}\} dA +$$

$$\frac{1}{2} \int_A \langle T_{Ref} \rangle [H_s]^{-1} \{T_{Ref}\} dA \tag{A-3}$$

and

$$||\Pi_{int}^{Ref} - \Pi_{int}^{FE}||^2 = \sum_{1}^{NELT} ||\Pi_{int}^{Ref} - \Pi_{int}^{FE}||_e^2 \tag{A-4}$$

$$||\Pi_{int}^{Ref} - \Pi_{int}^{FE}||_e^2 = \frac{1}{2} \int_A \langle \Delta N \rangle [H_m]^{-1} \{\Delta N\} dA +$$

$$\frac{1}{2} \int_A \langle \Delta M \rangle [H_b]^{-1} \{\Delta M\} dA +$$

$$\frac{1}{2} \int_A \langle \Delta N \rangle [H_{mb}]^{-1} \{\Delta M\} dA +$$

$$\frac{1}{2} \int_A \langle \Delta M \rangle [H_{mb}]^{-1} \{\Delta N\} dA +$$

$$\frac{1}{2} \int_A \langle \Delta T \rangle [H_s]^{-1} \{\Delta T\} dA \tag{A-5}$$

where

$$\langle \Delta N \rangle = \langle \langle N_{ref} \rangle - \langle N_h \rangle \rangle$$

$$\langle \Delta M \rangle = \langle \langle M_{ref} \rangle - \langle M_h \rangle \rangle \; ; \; \langle \Delta T \rangle = \langle \langle T_{ref} \rangle - \langle T_h \rangle \rangle \tag{A-6}$$

We integrate over the element area using Gauss point (2×2) in the reference mesh. From the result of each element of the target mesh, we have to calculate the values of $\langle N_h(\xi_I, \eta_I) \rangle$, $\langle M_h(\xi_I, \eta_I) \rangle$ and $\langle T_h(\xi_I, \eta_I) \rangle$ at Gauss points I (A-6) of each element in the reference mesh.

In the *s-norm* method, the errors are represented by plotting curves Log of E_S in term of Log L_k, where L_k represents an indicator of the element size in a mesh (in our work L_k is the element size for square elements and an average element size for distorted meshes). The theoretical convergence (energy) formula:

$$E_s \cong c L_k^{2p} \tag{A-7}$$

where c is a constant and p is the interpolation order. We use reference lines for Eq. (A-7) with $p = 1$ corresponding to a linear convergence.

References

[1] Kirchhoff G. Uber das Gleichgewicht und die Bewegung einer elastischen Scheibe. J Reine Angew Math 1950;40:51–8.

[2] Naghdi PM. On the theory of thin elastic shells. Q Appl Math 1957;14:369–80.

[3] Naghdi PM. Foundations of elastic shells theory. In: Sneddon IN, Hill R. Progress in Solid Mechanics; IV, Chapter 1. North-Holland; 1963.

[4] Naghdi PM. On a variational theorem in elasticity and its application to shell theory. J Appl Mech (ASME) 1964;31(4):647–53.

[5] Naghdi PM. The theory of shells and plate. Handbuch der Physik, VI, A2 (Flugge Ed.). Berlin: Springer Verlag; 1972.

[6] Reissner E. The effect of transverse shear deformation on the bending of elastic plates. J Appl Mech Eng ASME 1945;12:A69–77.

[7] Mindlin RD. Influence of rotator inertia and shear on flexural motion of isotropic elastic plates. J Appl Mech Eng 1951;18:31–8.

[8] Hughes TJR. The finite element method: Linear static and dynamic finite element analysis. Dover Publications Inc.; 2000.

[9] Belytschko T, Liu W, Moran B. Nonlinear finite elements for continua and structures. John Wiley & Sons Ltd.; 2000.

[10] Batoz J-L, Dhatt G. Modélisation des structures éléments finis: Poutres et Plaques. vol. 2. Hermes Science Publications; 1990.

[11] Batoz J-L, Dhatt G. Modélisation des structures éléments finis: Coques. vol. 3. Hermes Science Publications; 1992.

[12] Pawsey S, Clough R. Improved numerical integration of thick shell finite elements. Int J Numer Meth Eng 1971;3:575–86.

[13] Zienkiewicz O, Taylor R, Too J. Reduced integration technique in general analysis of plates and shells. Int J Numer Meth Eng 1974;3:275–90.

[14] Belytschko T, Ong J-J, Liu W, Kenedy J. Hourglass control in linear and non-linear problems. Comput Methods Appl Mech Eng 1984;43:251–76.

[15] Hughes TJR, Cohen M, Haroun M. Reduced and selective integration techniques in the finite element analysis of plates. Nucl Eng Des 1978;46:203–22.

[16] Hughes TJR, Taylor R, Kanoknukulchai W. A simple and efficient finite element for plate bending. Int J Numer Meth Eng 1977;11:1529–43.

[17] Malkus D, Hughes TJR. Mixed finite element methods-reduced and selective integration techniques: a unification of concepts. Comput Methods Appl Mech Eng 1978;15:63–81.

[18] Prathap G, Bhashyam G. Reduced integration and the shear-flexible beam element. Int J Numer Meth Eng 1982;18:172–8.

[19] Prathap G. The finite element method in structural mechanics. Dordrecht: Kluwer Academic Press; 1993.

[20] Stolarski H, Belytschko T. Membrane locking and reduced integration for curved element. J Appl Mech 1982;49:172–8.

[21] Adam C, Bouabdallah S, Zarroug M, Maitournam H. Improved numerical integration for locking treatment in isogeometric structural elements, Part I: beams. Comput Methods Appl Mech Eng 2014;279:1–28.

[22] Adam C, Bouabdallah S, Zarroug M, Maitournam H. Improved numerical integration for locking treatment in isogeometric structural elements, Part II: plates and shells. Comput Methods Appl Mech Eng 2015;284:106–37.

[23] Simo J, Rifai S. A class of mixed assumed strain methods and the method of incompatible modes. Int J Numer Meth Eng 1990;29:1595–638.

[24] Koschnick F, Bischoff M, Camprubi N, Bletzinger K-U. The discrete strain gap method and membrane locking. Comput Methods Appl Mech Eng 2005;194:2444–63.

[25] Bouclier R, Elguedj T, Combescure A. Locking free isogeometric formulations of curved thick beams. Comput Methods Appl Mech Eng 2012;245:144–62.

[26] Bouclier R, Elguedj T, Combescure A. Efficient isogeometric NURBS-based solid-shell elements: Mixed formulation and B-method. Comput Methods Appl Mech Eng 2013;267:86–110.

[27] Dvorkin EN, Bathe KJ. A continuum mechanics based four-node shell elements for general non-liner analysis. Eng Comput 1984;1:77–88.

[28] Lee PS, Bathe KJ. Development of MITC isotropic triangular shell finite elements. Comput Struct 2004;82(11):945–62.

[29] Lee Y, Lee PS, Bathe KJ. The MITC3+ shell element and its performance. Comput Struct 2014;138:12–23.

[30] Ko Y, Lee PS, Bathe KJ. A new MITC4+ shell element. Comput Struct 2017;182:404–18.

[31] Bletzinger KU, Bischoff M, Ramm E. A unified approach for shear-locking-free triangular and rectangular shell finite elements. Comput Struct 2000;75(3):321–4.

[32] Batoz J-L, Bathe KJ, Ho LW. A study of three-node triangular plate bending elements. Int J Numer Meth Eng 1980;15:1771–812.

[33] Batoz J-L, Ben Tahar M. Evaluation of a new thin plate quadrilateral element. Int J Numer Meth Eng 1982;18:1655–78.

[34] Batoz J-L, Lardeur P. A discrete shear triangular nine dof element for the analysis of thick to very thin plates. Int J Numer Meth Eng 1989;28:533–60.

[35] Lardeur P. Développement et evaluation de deux nouveaux éléments finis de plaques et coques composites avec influences du cisaillement transverse [Thèse de Doctorat]. France: Université de Technologie Compiègne; 1990.

[36] Batoz J-L, Katili I. On a simple triangular Reissner/Mindlin plate element based on incompatible modes and discrete constraints. Int J Numer Meth Eng 1992;35:1603–32.

[37] Ibrahimbegović A. Plate quadrilateral finite element with incompatible modes.

Commun Appl Numer Methods 1992;8:497–504.

[38] Ibrahimbegović A. Quadrilateral finite elements for analysis of thick and thin plates. Comput Methods Appl Mech Eng 1993;110:195–209.

[39] Ibrahimbegović A, Frey F. Stress resultant geometrically non-linear shell theory with drilling rotations. Part III: linearized kinematics. Int J Numer Meth Eng 1994;37:3659–83.

[40] Katili I. A new discrete Kirchhoff-Mindlin element based on Mindlin-Reissner plate theory and assumed shear strain fields - part I: An extended DKT element for thick-plate bending analysis. Int J Numer Meth Eng 1993;36:1859–83.

[41] Katili I. A new discrete Kirchhoff-Mindlin element based on Mindlin-Reissner plate theory and assumed shear strain fields - part II: An extended DKQ element for thick plate bending analysis. Int J Numer Meth Eng 1993;36:1885–908.

[42] Mahjudin M, Lardeur P, Druesne F, Katili I. Stochastic finite element analysis of plates with the certain generalized stresses method. Struct Saf 2016;61:12–21.

[43] Katili I, Hamdouni A, Rastandi JI, Millet O, Maknun IJ. Error estimation of plate bending problem using DKMQ element. Mod Mech Eng J 2012;2:47–55.

[44] Wong FT, Erwin, Richard A, Katili I. Development of the DKMQ element for buckling analysis of shear-deformable plate bending. Procedia Eng 2017;171:805–12.

[45] Katili I, Maknun IJ, Millet O, Hamdouni A. Application of DKMQ element for composite plate bending structures. Compos Struct 2015;132:166–74.

[46] Maknun IJ, Katili I, Purnomo H. Development of DKMT element for error estimation in composite plate structures. Int J Technol 2015;6(5):780–9.

[47] Rodrigues JD, Natarajan S, Ferreira AJM, Carrera E, Cinefra M, Bordas SPA. Analysis of composite plates through cell-based smoothed finite element and 4-noded mixed interpolation of tensorial components techniques. Comput Struct 2014;135:83–7.

[48] Xing YF, Wu Yang, Liu Bo, Ferreira AJM, Neves AMA. Static and dynamic analyses of laminated plates using a layer wise theory and a radial basis function finite element method. Compos Struct 2017;170:158–68.

[49] Thai HC, Ferreira AJM, Nguyen-Xuan H. Naturally stabilized nodal integration mesh free formulations for analysis of laminated composite and sandwich plates. Compos Struct 2017;178:260–76.

[50] Castellazzi G, Krysl P, Bartoli I. A displacement-based finite element formulation for the analysis of laminated composite plates. Compos Struct 2013;95:518–27.

[51] Alfano G, Auricchio F, Rosati L, Sacco E. MITC finite elements for laminated composite plates. Int J Numer Meth Eng 2001;50:707–38.

[52] Katili I, Batoz J-L, Maknun IJ, Hamdouni A, Millet O. The development of DKMQ plate bending element for thick to thin shell analysis based on Naghdi/Reissner/Mindlin shell theory. Finite Elem Anal Des 2014;100:12–27.

[53] Maknun IJ, Katili I, Millet O, Hamdouni A. Application of DKMQ24 shell element for twist of thin-walled beams: comparison with Vlasov theory. Int J Comput Methods Eng Sci Mech 2016;17(6):391–400.

[54] Irpanni H, Katili I, Maknun IJ. Development DKMQ shell element with five degrees of freedom per nodal. Int J Mech Eng Rob Res 2017;6:248–52.

[55] Kiendl J, Auricchio F, Hughes TJR, Reali A. Single-variable formulations and iso-geometric discretization for shear deformable beams. Comput Methods Appl Mech Eng 2015;284:988–1004.

[56] Katili I. Unified and integrated approach in a new Timoshenko beam element. Eur J Comput Mech 2017;26:282–308.

[57] Senjanović I, Vladimir N, Tomić M. An advanced theory of moderately thick plate vibrations. J Sound Vib 2013;332:1868–80.

[58] Thai HT, Nguyen TK, Vo TP, Ngo T. A new simple shear deformation plate theory. Compos Struct 2017;171:277–85.

[59] Katili I, Aristio R. Isogeometric Galerkin in rectangular plate bending problem based on UI approach. Eur J Mech A Solids 2018;67:92–107.

[60] Washizu K. Variational methods in elasticity and plasticity. 3rd ed. Pergamon Press; 1982.

[61] Ibrahimbegović A. Nonlinear solid mechanics: theoretical formulations and finite element solution methods. Springer; 2009.

[62] Katili I. Formulation et évaluation des nouveaux éléments finis pour l'analyse linéaire des plaques et coques de forme quelconque [Thèse Doctorat]. U.T.C; 1993.

[63] Bathe KJ, Dvorkin EN. A four-node plate bending element based on Mindlin-Reissner plate theory and a mixed interpolation. Int J Numer Meth Eng 1985;21:367–83.

[64] Ibrahimbegović A, Taylor RL, Wilson EL. A robust quadrilateral membrane finite element with drilling degrees of freedom. Int J Numer Meth Eng 1990;30:445–57.

[65] Srinivas S. A refined analysis of composite laminates. J Sound Vib 1973;30(4):495–507.

[66] Pagano NJ. Exact solutions for rectangular bidirectional composites and sandwich plates. J Compos Mater 1970;4:20–34.

[67] Pagano NJ, Hatfield SJ. Elastic behaviour of multilayered bidirectional composites. AIAA J 1972;10:931–3.

[68] Varadan TK, Bhaskar K. Bending of laminated orthotropic cylindrical shells – An elasticity approach. Compos Struct 1991;17:141–56.

[69] Chapelle D, Bathe KJ. The finite element analysis of shells fundamentals. 2nd ed. Springer; 2011.

[70] Hiller JF, Bathe KJ. Measuring convergence of mixed finite element discretization: an application to shell structures. Comput Struct 2003;81:639–54.

[71] Ren JG. Analysis of simply supported laminated circular cylindrical shell. Comput Struct 1989;11:277–92.

[72] Bathe KJ, Iosilevich A, Chapelle D. An inf-sup test for shell finite elements. Comput Struct 2000;75:439–56.

[73] Chapelle D, Bathe KJ. Optimal consistency errors for general shell elements. C.R. Acad. Sci. Paris, Serie I 2001;332:771–6.

[74] Ko Y, Lee PS, Bathe KJ. The MITC4+ shell elements and its performance. Comput Struct 2016;169:57–68.